NAVAL POSTGRADUATE SCHOOL
Monterey, California

THESIS

Survey of Trapped Plasmas at the Earth's Magnetic Equator

by

Peter G. Braccio

December 1991

Thesis Advisor: R. C. Olsen

REPORT DOCUMENTATION PAGE

1a. REPORT SECURITY CLASSIFICATION Unclassified	1b. RESTRICTIVE MARKINGS
2a. SECURITY CLASSIFICATION AUTHORITY	3. DISTRIBUTION/ AVAILABILITY OF REPORT Approved for public release; distribution is unlimited.
2b. DCLASSIFICATION/DOWNGRADING SCHEDULE	
4. PERFORMING ORGANIZATION REPORT NUMBER(S)	5. MONITORING ORGANIZATION REPORT NUMBER(S)
6a. NAME OF PERFORMING ORGANIZATION Naval Postgraduate School 6b. OFFICE SYMBOL *(If Applicable)* 33	7a. NAME OF MONITORING ORGANIZATION Naval Postgraduate School
6c. ADDRESS *(city, state, and ZIP code)* Monterey, CA 93943-5000	7b. ADDRESS *(city, state, and ZIP code)* Monterey, CA 93943-5000
8a. NAME OF FUNDING/SPONSORING ORGANIZATION 6b. OFFICE SYMBOL *(If Applicable)*	9. PROCUREMENT INSTRUMENT IDENTIFICATION NUMBER
8c. ADDRESS *(city, state, and ZIP code)*	10. SOURCE OF FUNDING NUMBERS PROGRAM ELEMENT NO. / PROJECT NO. / TASK NO. / WORK UNIT ACCESSION NO.

11. TITLE *(Include Security Classification)*
SURVEY OF TRAPPED PLASMAS AT THE EARTH'S MAGNETIC EQUATOR

12. PERSONAL AUTHOR(S)
Braccio, Peter G.

13a. TYPE OF REPORT	13b. TIME COVERED	14. DATE OF REPORT *(year, month,day)*	15. PAGE COUNT
Master's Thesis	FROM TO	December 1991	89

16. SUPPLEMENTARY NOTATION
The views expressed in this thesis are those of the author and do not reflect the official policy or position of the Department of Defense or the U.S. Government.

17. COSATI CODES			18. SUBJECT TERMS *(continue on reverse if necessary and identify by block number)*
FIELD	GROUP	SUBGROUP	Equatorially Trapped Plasma, Plasmapause, AMPTE, Ion Distributions, Electron Distributions, Survey of Low Energy Trapped Particles

19. Abstract (Continue on reverse if necessary and identify by block number)

Analysis of data from the HPCE experiment on the AMPTE/CCE satellite established probability distributions for trapped ions and electrons. Trapped 150 eV electrons occurred primarily in the dawn to noon local time sector, centered at L = 6. Trapped 50-150 eV ion distributions show strong L versus local time dependence, but are primarily found on the dayside (the dusk sector was not sampled for ions in this survey). This local time dependence appears to reflect the L versus local time dependance of the plasmapause. The regions of peak occurrence probability for trapped ions were mutually exclusive with the high probability regions of trapped electrons. This offset in the location of trapped plasma species was seen frequently on a daily basis as well as in the statistical survey.

20. DISTRIBUTION/AVAILABILITY OF ABSTRACT	21. ABSTRACT SECURITY CLASSIFICATION
[X] UNCLASSIFIED/UNLIMITED [ ] SAME AS RPT. [ ] DTIC USERS	Unclassified

22a. NAME OF RESPONSIBLE INDIVIDUAL	22B. TELEPHONE (INCLUDE AREA CODE)	22c. OFFICE SYMBOL
Richard C. Olsen	(408) 646-2019	PH/Os

Approved for public release; distribution is unlimited.

Survey of Trapped Plasmas at the Earth's Magnetic Equator

by

Peter G. Braccio
Lieutenant, United States Navy
B.A., Boston University, 1985

Submitted in partial fulfillment of the requirements for
the degree of

MASTER OF SCIENCE IN PHYSICS

from the

NAVAL POSTGRADUATE SCHOOL
December 1991

Author: _____
Peter G. Braccio

Approved by: _____
R. C. Olsen, Thesis Advisor

_____
S. Gnanalingham, Second Reader

_____
K. E. Woehler, Chairman, Department of Physics

ABSTRACT

Analysis of data from the HPCE experiment on the AMPTE/CCE satellite established probability distributions for trapped ions and electrons. Trapped 150 eV electrons occurred primarily in the dawn to noon local time sector, centered at L= 6. Trapped 50-150 eV ion distributions show strong L versus local time dependence, but are primarily found on the dayside (the dusk sector was not sampled for ions in this survey). This local time dependence appears to reflect the L versus local time dependance of the plasmapause. The regions of peak occurrence probability for trapped ions were mutually exclusive with the high probability regions of trapped electrons. This offset in the location of trapped plasma species was seen frequently on a daily basis as well as in the statistical survey.

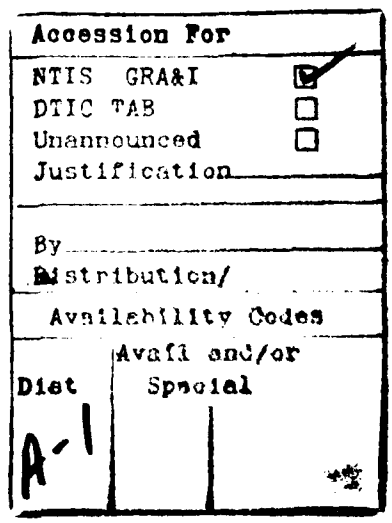

TABLE OF CONTENTS

LIST OF FIGURES

LIST OF TABLES

ACKNOWLEDGMENTS

The author wishes to express his gratitude to Professor R. C. Olsen, without whose help and advice this work would not have been possible.

The author also wishes to thank Doctor David M. Klumpar, of the Lockheed Palo Alto Research Laboratory, for the use of the data presented in this paper.

I. INTRODUCTION

Equatorially trapped plasmas are ion and electron distributions trapped within a few degrees of the Earth's magnetic equator. These trapped plasma distributions were defined by the initial observations by Olsen (1981). Ion and electron distributions with highly anisotropic pitch angle distributions, peaked at 90° pitch angle, were observed at energies from a few eV to hundreds of eV, near geosynchronous orbit. These trapped distributions are of interest as indications of basic wave particle interactions, and as an intermediate process in plasmasphere filling.

The energy - pitch angle distribution indicates the wave particle interaction aspect of these plasmas. This is indicative of perpendicular acceleration ($T_{perp} > T_{par}$), and quasi-linear diffusion (flat diffusion at low energy). Though not yet proven, there are indications of a correspondence between equatorially trapped plasmas and Bernstein mode waves (equatorial noise) and electron cyclotron harmonics (Gurnett, 1976 and Kurth *et al.*, 1979).

The plasmasphere filling role is indicated by the correspondence between the plasmapause region and the location of equatorially trapped ion distributions (Horwitz *et al.*, 1981). The variation in pitch angle structure with latitude also suggests this role (Olsen *et al.*, 1987).

There have been previous surveys of equatorially trapped plasmas. Olsen *et al.* (1987) surveyed DE 1/RIMS (ion) data for 0 - 100 eV. Sagawa *et al.* (1987) surveyed the DE 1/EICS (ion) data for 0 - 1 keV. Both surveys of equatorially trapped plasma were limited in altitude by the DE 1 orbit, which had apogee at L = 4.7. Both of these surveys also lacked complementary electron data.

In this work, ion and electron data for AMPTE/CCE will be surveyed out to 8.8 R_E. Additionally, this data will be surveyed in stages of increasingly more stringent selection criteria for the equatorially trapped plasmas. This will show if the location of the trapped plasma distribution is affected by the criteria used to define it. This will provide a more complete look at the trapped ion distribution and a first survey of trapped electrons.

II. BACKGROUND

A. THE PLASMASPHERE

A magnetosphere is the region around a magnetized planetary body in which that body's magnetic field plays the dominant role in defining the behavior of charged particles. It's outer boundary, the magnetopause, occurs where the solar wind, and the magnetic field in the solar wind, become dominant. This boundary occurs, in the Earth's magnetic plane on the sunward side, at approximately 10 Earth radii (roughly 63,750 km). The location of this boundary is determined by a balance between the pressure exerted by the solar wind and the obstacle formed by the Earth's magnetic field. During active times, the magnetopause has been observed as close as 5 geocentric Earth radii (R_E). The inner boundary of the magnetosphere occurs at the top of the ionosphere. This boundary can be taken as occurring at an altitude of 1000 km or 1.16 R_E. (Parks, p.7)

As can be seen in Figure 1, the Earth's magnetosphere is highly asymmetric. While the sunward boundary is located at approximately 10 R_E, the Earth's magnetic tail has been seen to extend beyond 200 R_E on the nightside. The length and shape of the magnetic tail again depends on the interaction between the geomagnetic field and the solar wind. (Parks, pp. 7-8)

For our purposes, the major components of the magnetosphere are the plasmasphere, the plasmasheet, and the plasmapause. The plasmasphere is the region of the magnetosphere that is closest to the Earth. It begins just above the ionosphere, at low to mid-latitudes. The plasmasphere extends in altitude to between 3 and 5 R_E, in the equatorial plane, and between $\pm$ 60° magnetic latitude.

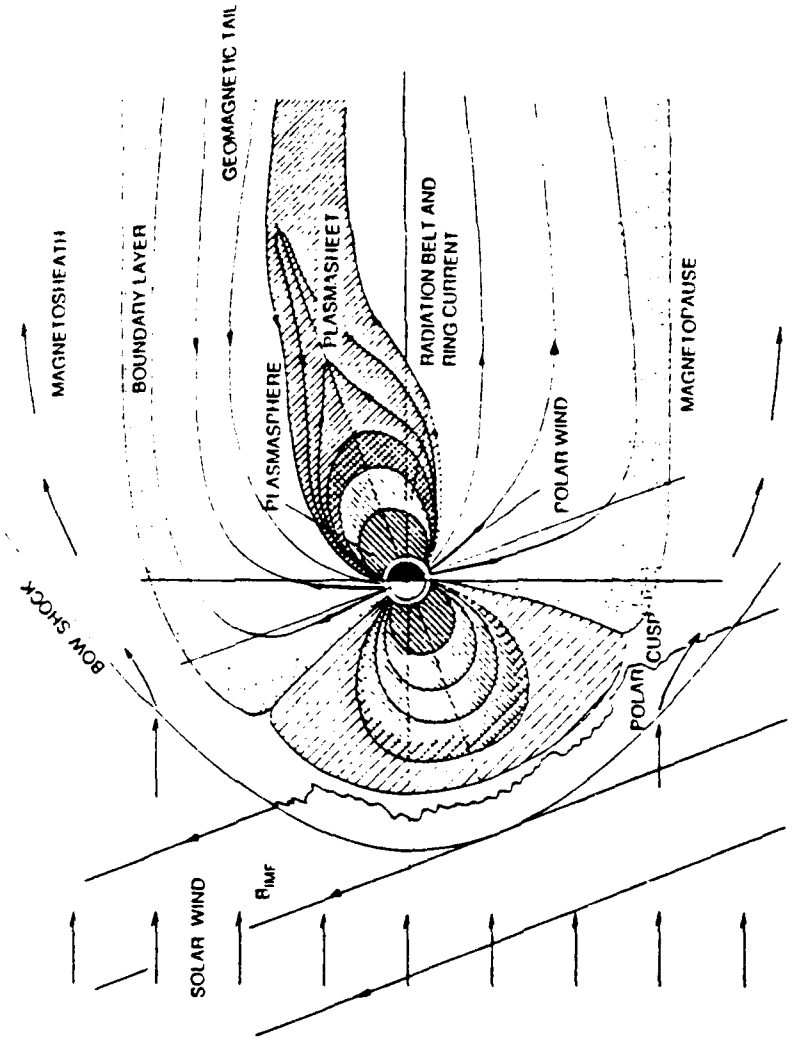

A schematic diagram of Earth's magnetosphere in the noon-midnight plane. The basic particle and magnetic field features are representative of other planetary magnetospheres although the details can be different.

Figure 1. The Earth's Magnetosphere

The plasmasphere corotates with the Earth and particles in this region are affected by the Earth's corotational Electric field. (Parks, pp. 11 and 73)

This region contains plasma, ionized atoms and electrons, with densities of 10^{2}-10^{4} cm^{-3}. Characteristic ion and electron energies are on the order of 1 eV at 4.5 R_E. The density of the plasmasphere decreases with altitude. In general, density in this region experiences a gradual drop proportional to the fourth power of the McIlwain L parameter (a measure of altitude based on magnetic field lines that will be discused later). This is illustrated in Figure 2. (Chappell *et al.*, 1970)

At approximately 3 to 5 Earth radii, again depending on the magnetic activity history, the plasmapause is encountered. This is a transition region for the plasma in which plasma energies sharply increase (Parks, pp. 231 and 502). There is also a drop in density, which generally is very sharp, that is used to define the inner boundary of the plasmapause (figure 3) (Harris *et al.*, 1970).

The above aspects of the plasmasphere can be further illustrated using (relatively) more modern data from ISEE 1 total electron density measurements obtained from observations of plasma waves. Figure 4a shows density versus L, with a solid line at 100 x $(L/4.5)^{-4}$ superimposed. The plasmapause is at L = 4.8, 1700 local time. The plasma density outside the plasmapause continues to drop as L^{-4}. This characteristic of the plasma density profile can more easily be seen if the data are normalized by L^{4}, as in Figure 4b. (Olsen, 1992)

The plasmasphere density is dependent on magnetic activity. A large magnetic storm can effectively push the plasmapause in to less than 3 R_E. Figure 3 shows the effects of magnetic activity on density and location of the plasmapause. Magnetic intensity increases from a low in the upper left panel in the figure to a maximum in the lower right hand panel. (Harris *et al.*, 1970)

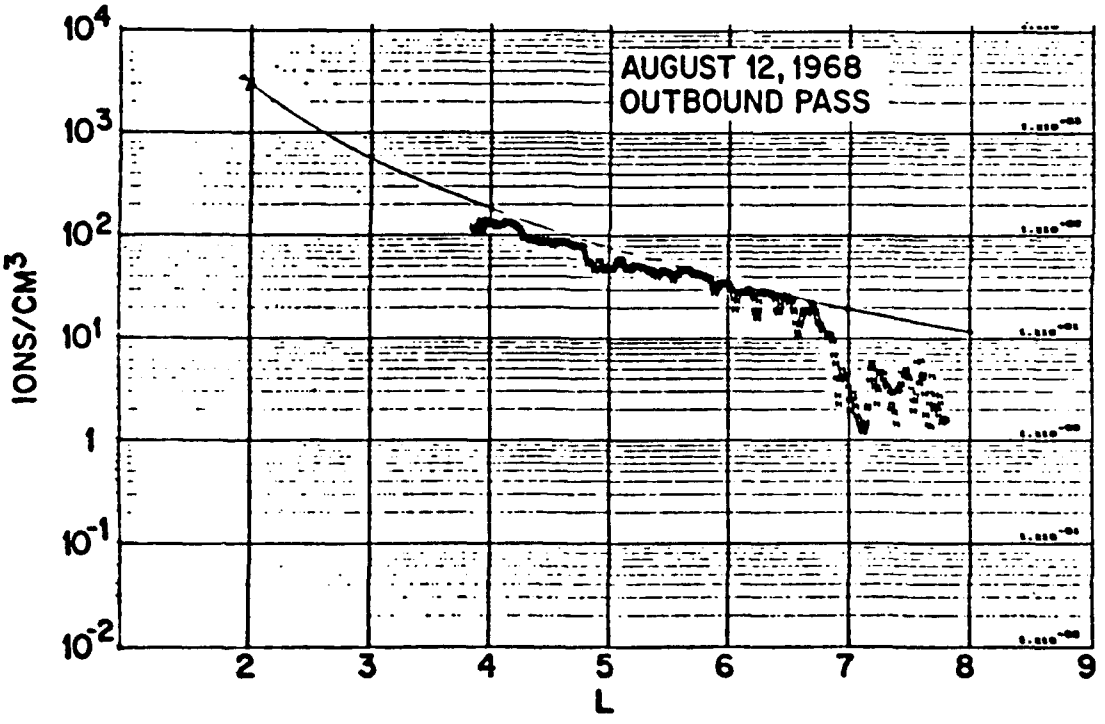

Figure 2. Plasma Density L Dependance

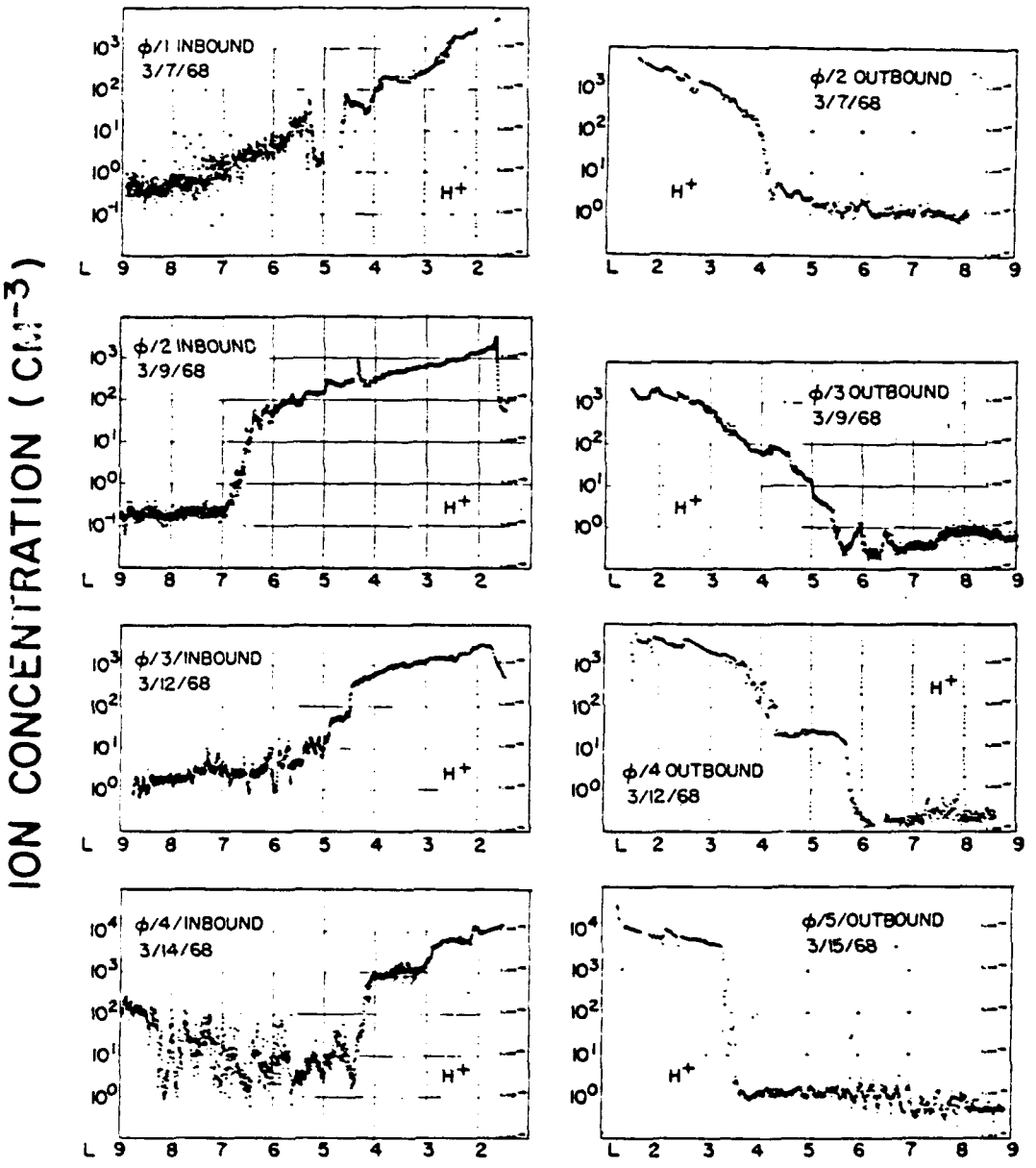

Composite of the first four H^+ ion concentration profiles for the inbound and outbound passes of OGO 5.

Figure 3. Plasmapause Magnetic Activity Dependence

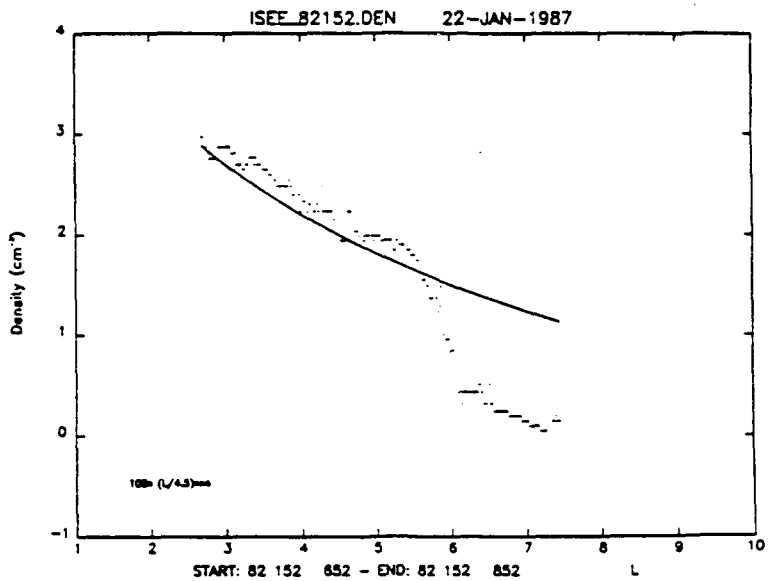

a.

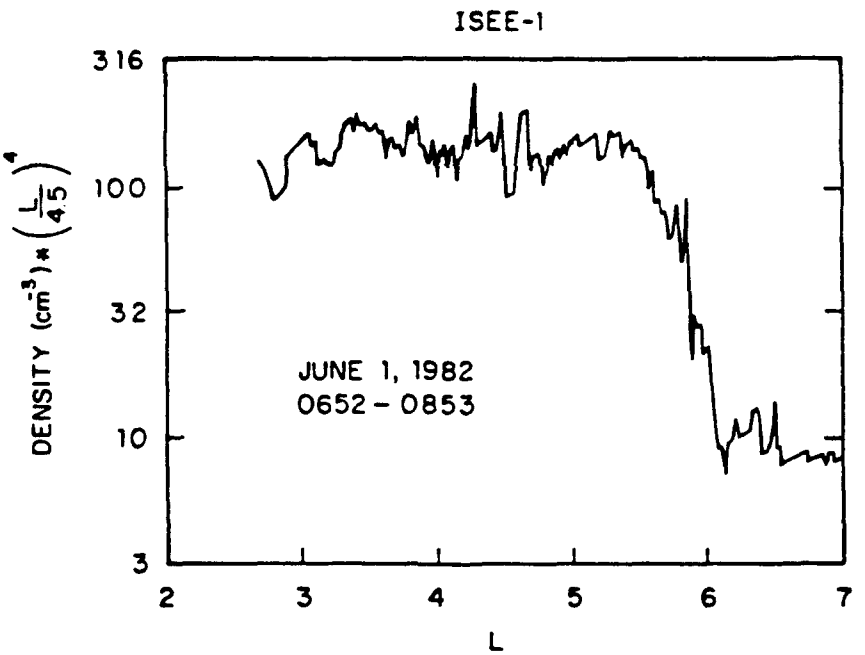

b.

Figure 4. Plasma Density L Dependance - Normalized

The storm-time electric field strips away the plasma at higher altitudes, as the plasma is convected to the magnetosphere. This region is then refilled from the ionosphere after the storm-time field relaxes. The process, termed the polar wind, is driven by ambipolar diffusion after the electric field relaxes back to a steady state value of ≈ 1 mV/m. This diffusion process calls for electrons to leave the upper ionosphere, probably driven by photoemission, and move along the geomagnetic field lines. The resulting ambipolar electric field, caused by the displacement between the electrons and O^+ in the upper atmosphere, causes lighter ions, such as $H^+$and He^+, to be dragged up the field lines after the electrons. This 'polar wind' results in a refilling rate of 1 to 10 ions/cm^3 per day. (Horwitz, 1983)

On the nightside the plasmasphere is bounded by plasma sheet, a region of low density, hot plasma (with densities on the order of 1 cm^{-3} and characteristic energies of 1-10 keV). The corresponding plasmapause for this region is very distinct and the transition from plasmasphere to plasmasheet takes place rather quickly. This is not the case for the region that extends from just before dawn until just after dusk local time, on the dayside. (Parks, pp. 231 and 502)

On the sunward side of the Earth, the plasmapause is a region that can be as much as 1 R_E in width. Additionally, there is usually no sharp distinction corresponding to its inner and outer boundaries during this local time period (Parks, p. 231). Therefore, it is usually a matter of judgement as to which region you are studying.

The region between the dayside plasmapause and the magnetopause is also ill defined. It is not clear whether the plasmasheet encircles the Earth and occupies this region. While there is no known reason why this should not be the case, the plasma observed in this region does not display the characteristics of that which is found in

the nightside plasmasheet. This has led to questions concerning the plasma filling mechanism for this region as well as to questions of where the plasma in this region comes from.

In the dusk region there is an additional asymmetry as seen in Figure 5. This dusk bulge is the result of interaction between the corotational electric field of the plasmasphere and the cross tail electric field induced by the solar wind. The corotational field is the result of the charged particles rotating with the Earth while trapped in its geomagnetic field and is directed radially inward toward the Earth. The cross tail electric field is induced by the solar wind's interaction with the Earth's magnetic field. This cross tail field is in the dawn-dusk direction in the equatorial plane of the magnetotail. The sum of these two electric fields results in a series of equipotential contours which mirror the dusk bulge (figure 6). (Parks, pp. 231-236)

B. THEORY

The force experienced by a charged particle in an electric and magnetic field is given by Lorentz's law:

(1) $$\underline{F} = q\,(\underline{E} + \underline{v} \times \underline{B})$$

In the plasmasphere the contribution of the electric field is primarily to add a small drift, which can be ignored in the context of our studies. Therefore, the force on the particle depends only on its component of velocity that is perpendicular to the magnetic field line, v_{perp}, and the magnitude of the magnetic field.

The magnitude of the Lorentz force is then given as:

(2) $$F = q\, v_{perp}\, B$$

and its direction is always perpendicular to both the magnetic field line and the particle's velocity vector. The Lorentz force does not affect the particle's velocity in the direction parallel to the electric field, v_{par}.

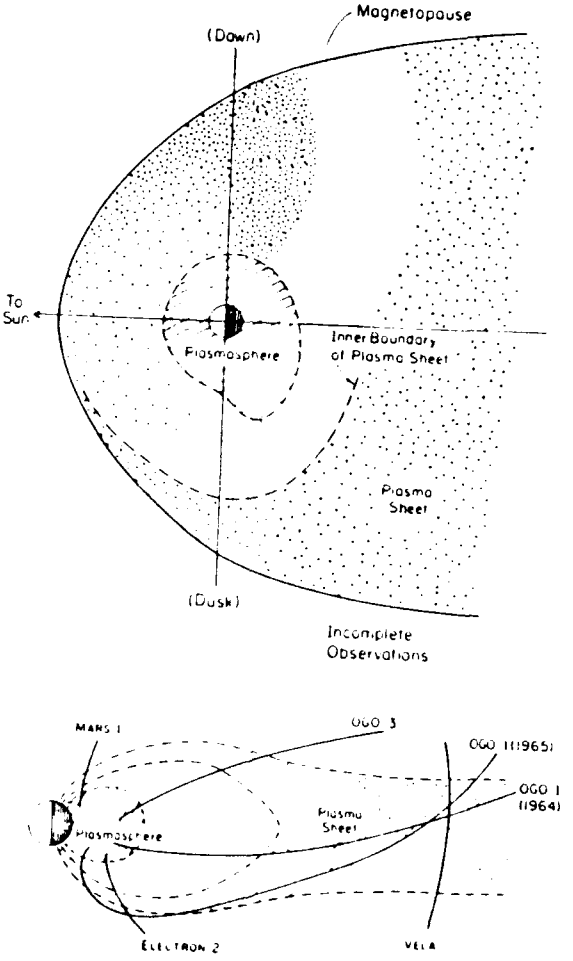

Figure 5. The Dusk Bulge

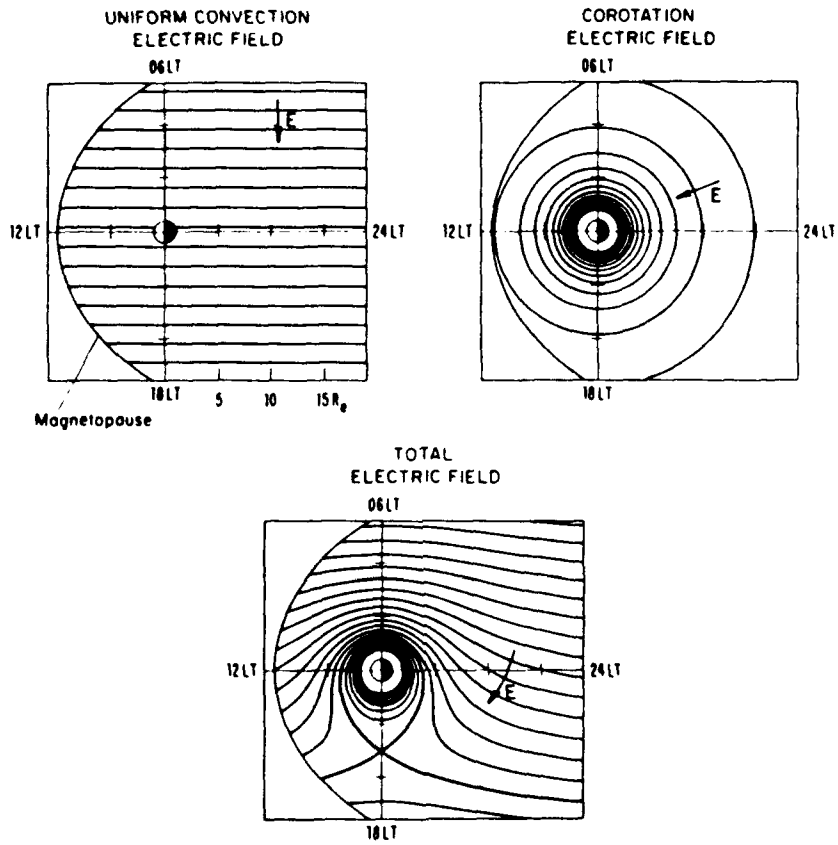

Equipotential contours for the magnetospheric electric field in the equatorial plane. Upper left: first-order approximation for the convection electric field E_c as uniform. The contours are spaced 3 kV apart for $E_c = 2.5 \times 10^{-4} V$ m^{-1}. Upper right: the corotation electric field, contours spaced 3 kV apart. Lower: sum of convection and corotation electric fields. The heavy contour separates the closed and open convection regions. (From Lyons and Williams, 1984)

Figure 6. Magnetosphere's Electric and Magnetic Fields

The particle's speed remains unchanged by the Lorentz force, since the force is perpendicular to the motion, hence it must move in a circle around the field line. Therefore, equating equation 2 with the formula for uniform circular motion gives:

(3) $$r_c = \frac{m v_{perp}}{qB}$$

where r_c is the cyclotron radius. (Parks, pp. 86-87)

The Earth's magnetic field lines converge at both the north and south magnetic poles, and the field strength increases with latitude. Because of this, there is an additional force that acts upon the charged particle. This force can be expressed as:

(4) $$\underline{F} = - \mu \nabla B \qquad \mu = \frac{m v^2_{perp}}{q B}$$

where μ is the magnetic moment. Because the gradient in the magnetic field is parallel to the direction of the field line it can be seen that this force is directed along the field line. Since this force is directed parallel to the particle's parallel velocity component, it will obviously affect the particle's velocity. From Lentz's law, it can be shown that μ is invariant. (Parks, pp. 89-90)

Since μ is invariant, v_{perp} must increase as B is increased. For this to happen v_{par} must decrease since $v^2_{perp} = v^2 - v^2_{par}$ (from conservation of energy). Therefore, given a large enough B, there will come a point where $v_{par} = 0$. At this point v_{perp} will equal v, and the particle will mirror back along the field line (figure 7) (Glasstone, 1967). (Notice that the gyroradius also gets smaller as the particle approaches the mirror point as a result of its v_{perp} dependance.)

For a particle that mirrors, equation 4 then leads to:

(5) $$\frac{m v^2_{perp\,o}}{2 B_o} = \frac{m v^2_{perp\,m}}{2 B_m}$$

where subscript o refers to values at the equator and m to those at the mirror point.

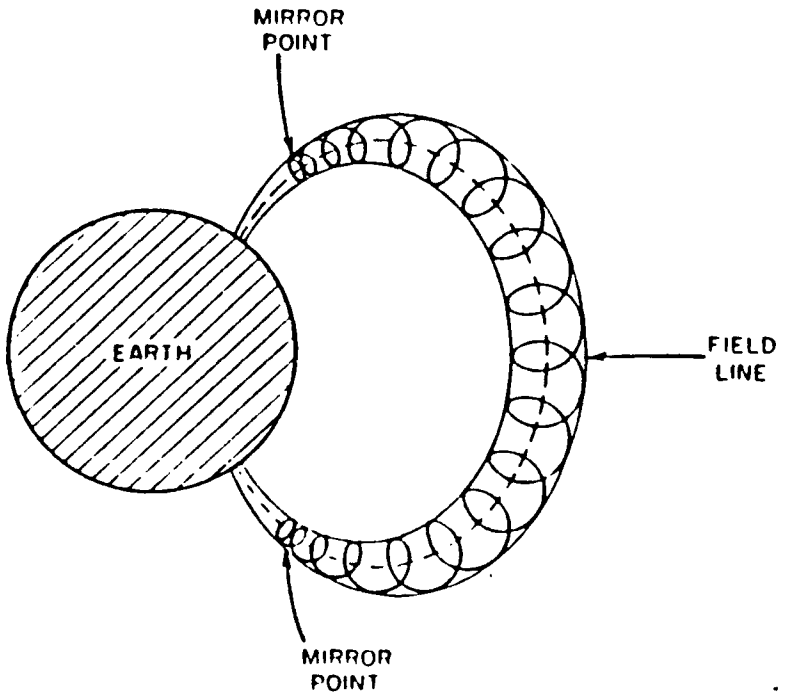

Figure 7. Path of Mirroring Particle

Rearranging equation 5 gives:

$$\frac{B_o}{B_m} = \frac{v^2_{perp\ o}}{v^2_{perp\ m}} = \frac{v^2_{perp\ o}}{v^2_o} \tag{6}$$

Defining the pitch angle of a particle, α, to be the angle between velocity vector of the particle and the magnetic field line gives $v_{perp} = v \sin \alpha$. Plugging this into equation 6 gives:

$$\frac{B_o}{B_m} = \sin^2 \alpha_o \tag{7}$$

which states that all particles with a pitch angle α_o will mirror at the location defined by $B = B_m$. Particles with $\alpha > \alpha_o$ will mirror at lower latitudes. (Parks, pp. 111-112)

The magnitude of the Earth's magnetic field is given according to:

$$B = \frac{B_{os}\sqrt{4 - 3\cos^2 \lambda}}{L^3 \cos^6 \lambda} \tag{8}$$

where B_{os} is the magnitude of the Earth's magnetic field on the Earth's surface at the magnetic equator, λ is the magnetic latitude, and L is the McIlwain L parameter (Parks, p. 54). The McIlwain L parameter is a variable, given in units of Earth radii, used to label magnetic field lines with relation to where they cross the plane of the magnetic equator. Its value is given by

$$L = r / \cos^2 \lambda \tag{9}$$

where r is the distance from the Earth's center, in R_E, to the field line at the magnetic equator (Parks, p. 115).

Substituting equation 8 into equation 7 gives:

$$\sin^2 \alpha_o = \frac{\cos^6 \lambda_m}{\sqrt{4 - 3\cos^2 \lambda_m}} \tag{10}$$

Therefore, by defining an equatorially trapped plasma to mirror at a magnetic latitude of $\pm$ 10° or less, this requires that a charged particle have a pitch angle

greater than 69°, at the equator, in order to be equatorially trapped (figure 8). It is these trapped particles that will be investigated in this paper.

C. PREVIOUS OBSERVATIONS

Thermal plasma pitch angle distributions seem to have been first studied by Horwitz and Chappell (1979) and Comfort and Horwitz (1980). These authors used electrostatic analyzer data to study ion pitch angle distributions at geosynchronous orbit, using ATS 6 data taken in 1974. The surveys dealt with data taken at 10.5° off the magnetic equator.

Comfort and Horwitz (1980) observed two important aspects of ion pancake distributions (peak flux near 90° pitch angle). The first was that the occurrence probability for the pancake component of the ion distribution was local time and energy dependant. The highest probability of occurrence occurred in the lowest energy channel (20 - 40 eV) studied and for local times between 1400 and 1800. Pancake distributions were seen 42% of the time in this sector for ions of that energy.

The second was that Comfort and Horwitz observed that field aligned ions and ions with 90° pitch angle seem to be anti-correlated. Figure 9 shows that there is a decrease in the occurrence probability of field aligned ions when there is a peak in the pancake occurrence probability.

Horwitz *et al.* (1981) studied pancake distributions in low energy ($\leq$ 100 eV) ion data obtained from the ISEE 1 mass spectrometer. These H^+ distributions were often found in the vicinity of the plasmapause (figure 10), and usually just inside the plasmapause. Horwitz *et al.* also observed that the pancake distribution was often seen in the presence of colder, isotropic plasma.

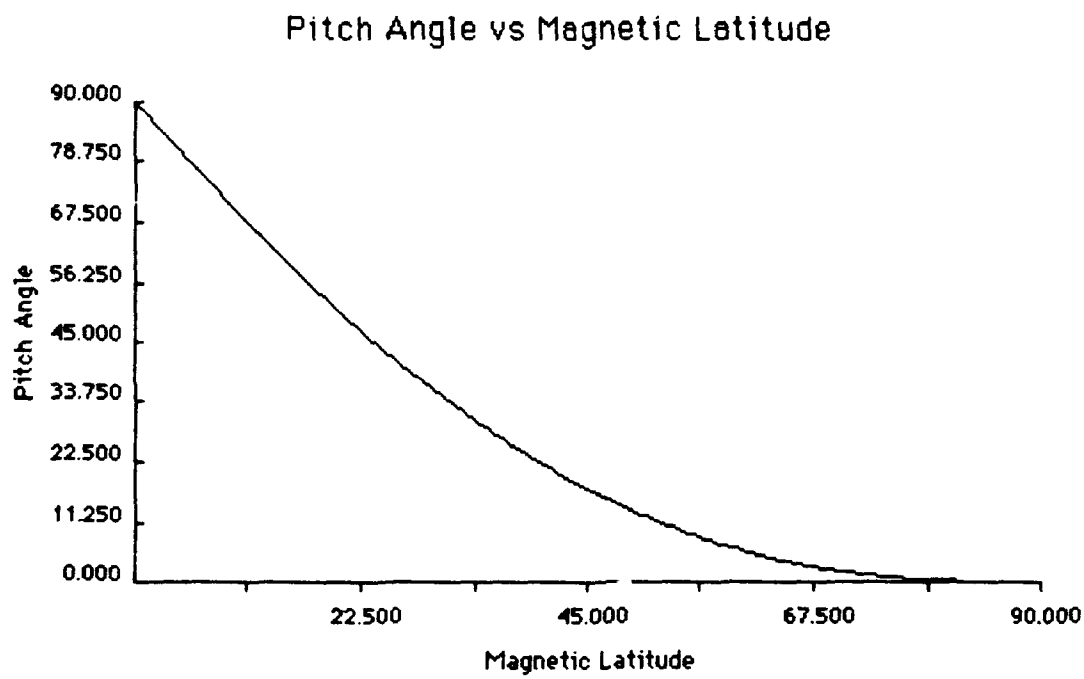

Figure 8. Pitch Angle verses Mirror Latitude

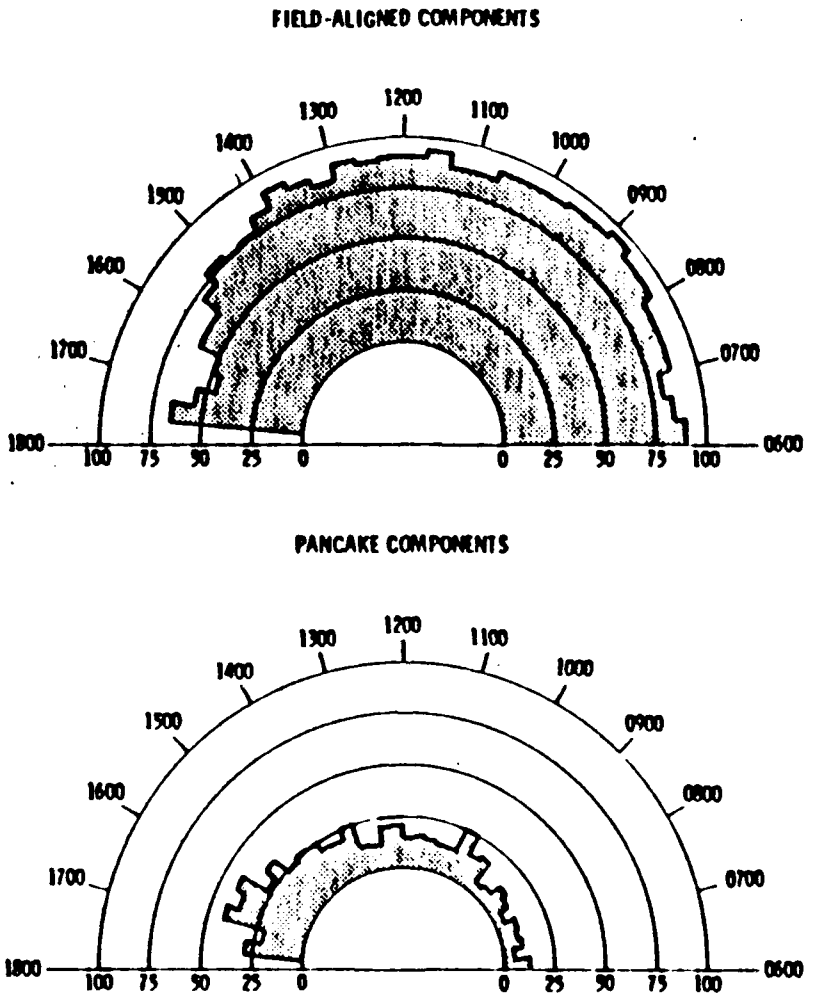

Total percent occurrence frequencies for ion pitch angle distributions having designated components, as functions of local time.

Figure 9. Field Aligned and Pancake Trapped Ion Distributions

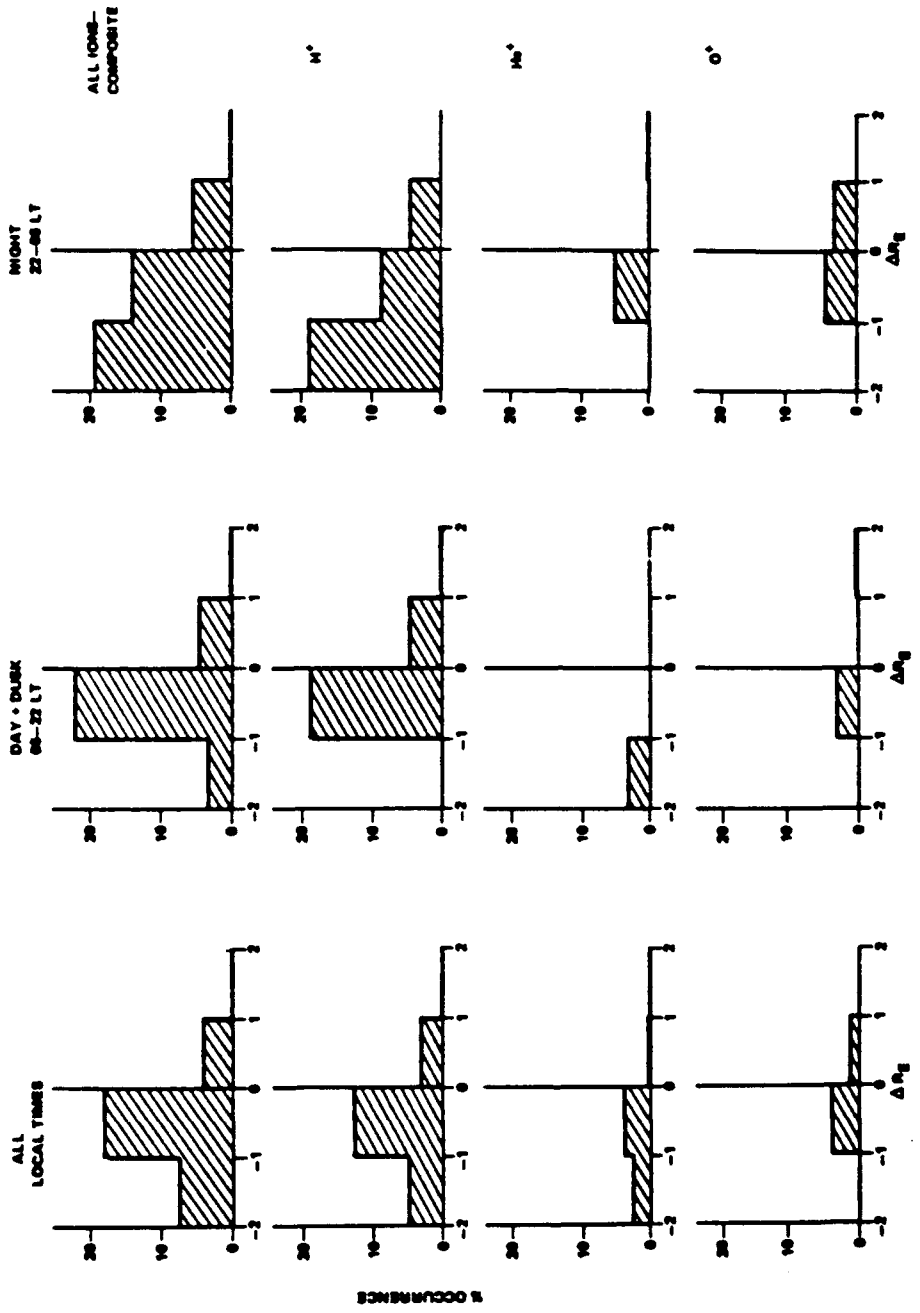

Fig. 11. Occurrence of frequencies of pancake distributions for inside and outside 'sharp' plasmapause in 1 R_E bins around the sharp plasmapause position, based on time as a measure.

Figure 10. Trapped Ion Distribution

With Relation to the Plasmapause

Olsen (1981) observed a thermal plasma population, trapped within a few degrees of the magnetic equator, using electrostatic analyzer data from the SCATHA satellite. Figure 11 shows the ion count rate, for various ion energies, as a function of pitch angle. The data for this plot was taken at the equator at approximately 1000 local time and 5.5 R_E. This figure clearly shows a trapped distribution, centered at 90° and 270° pitch angle, for ions of energies 11 to 103 eV and, to a lesser extent, for those at 523 eV. The 900 eV ions do not show evidence of a trapped distribution. This figure also shows a well defined loss cone for the three highest energies.

Olsen observed a like distribution in the electron data (figure 12). A source cone, centered at 0° and 180° pitch angles, was seen in the 41 eV electron flux concurrent with the trapped distribution at higher energies. This led to speculation that the field aligned particles were the (ionospheric) plasma source, and these particles were subsequently heated in the transverse direction. Note that the count rates in the last two figures are scaled differently for different energy levels in order to facilitate presentation of the data.

Figure 13, from Olsen (1981), shows a plot of count rate versus energy (in eV). The trapped electron distribution is seen to exist in the 50 to 1000 eV range, corresponding to temperatures of 100 - 200 eV and densities of 1 - 10 cm^{-3}. The trapped ions show a peak in the 20 to 200 eV range. This corresponds to temperatures of 20 to 50 eV and densities of 1 - 10 cm^{-3}.

Sagawa *et al.* (1987) observed a local time dependence in the location of the trapped ions in data from the Dynamics Explorer (DE) 1 satellite. Sagawa *et al.* additionally saw that the trapped ions were composed primarily of H^+ ions and that

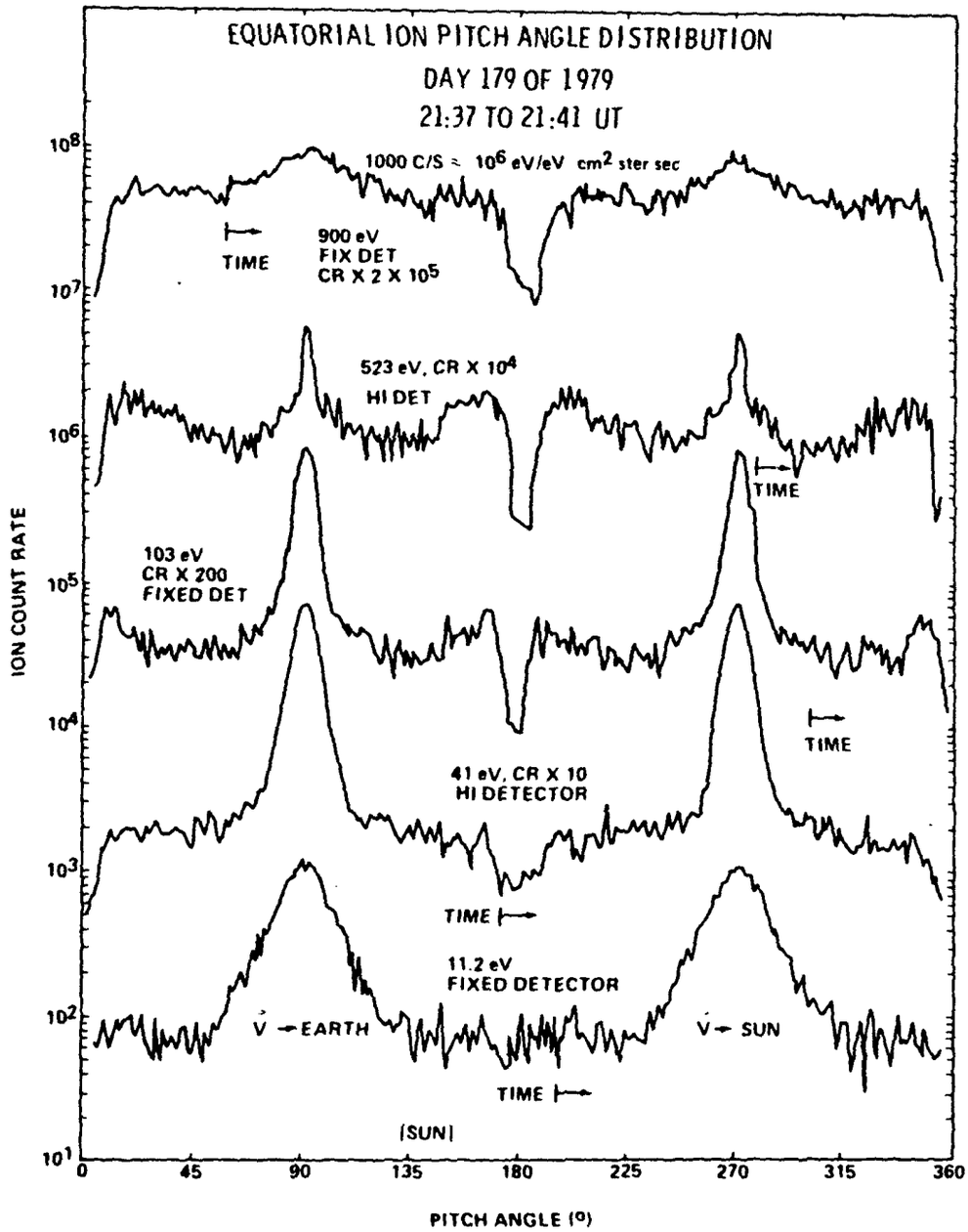

Ion pitch angle distributions at the equator for day 179 of 1979. Data are plotted from the FIX and HI detectors at 11, 41, 193, 523, and 900 eV. Fluxes are scaled by increasing factors to keep them from overlapping. Maximum values, with increasing energy are 1150 c/s, 7300 c/s, 4200 c/s, 550 c/s, and 540 c/s. The 0°-180° range corresponds to looking sunward, with 0° corresponding to looking south.

Figure 11. Ion Pitch Angle Distribution

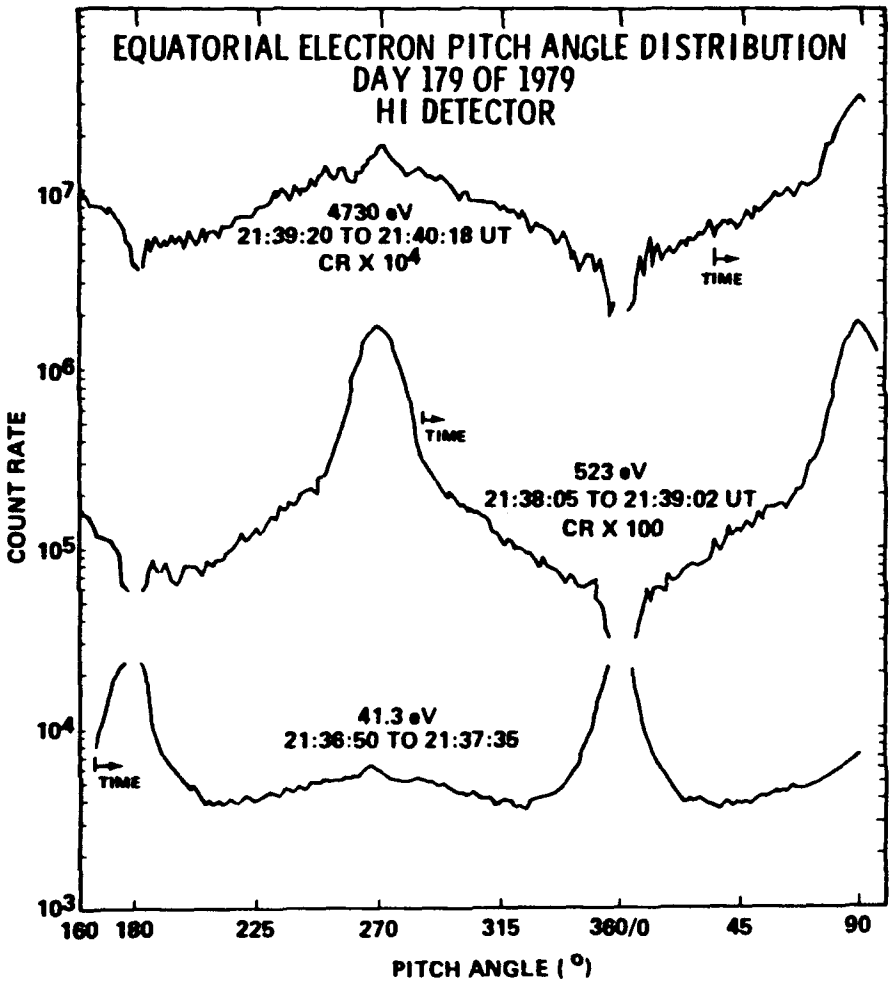

Electron pitch angle distributions at the equator for day 179 of 1979. Data are plotted from the HI detector at 41, 523, and 4730 eV. Pitch angle conventions are as in Figure 7.

Figure 12. Electron Pitch Angle Distribution

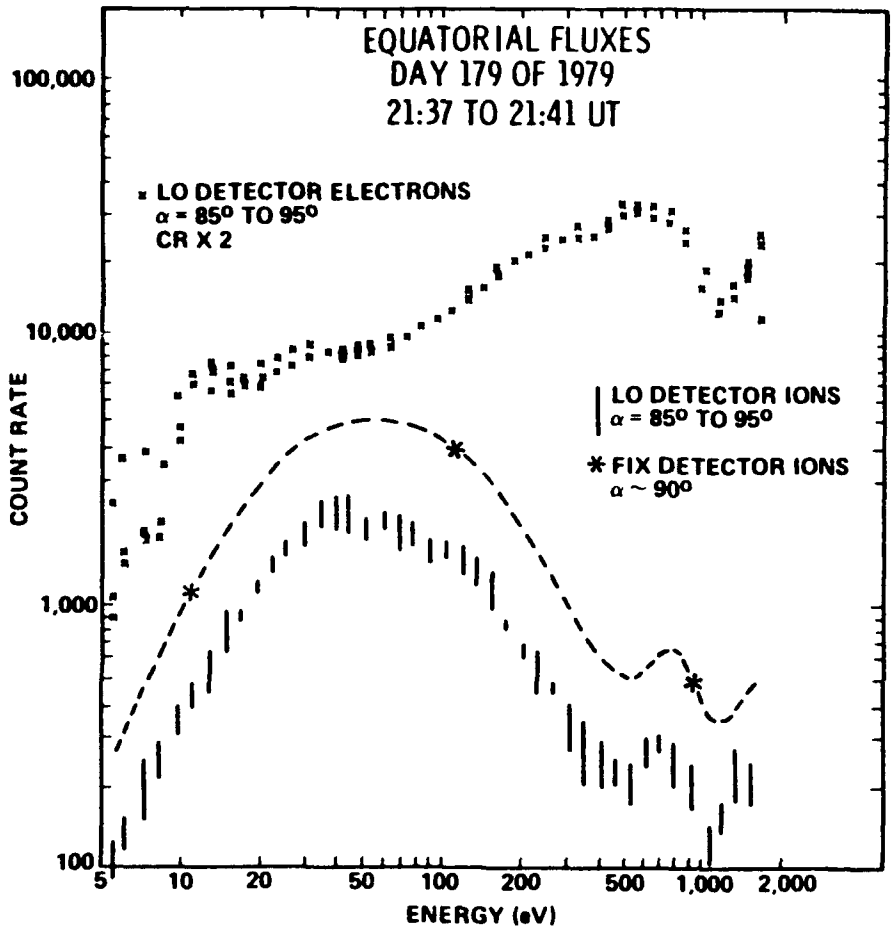

Ion and electron count rates as a function of energy from the LO detector near 90° pitch angle for day 179 of 1979. The electron count rate has been scaled by a factor of 2. The count rates from the FIX detector dwells were selected at their maxima (90° pitch angle). The difference between the LO and FIX ion data reflects degradation of the spiraltrons for the LO ion detector. The LO count rate curve has been traced and moved up to overlap the FIX detector data (about a factor of 2). The peak in ion count rate at 700 eV is a local maximum in the distribution function as well (see Figure 10).

Figure 13. Energy Relations of Trapped Plasmas

these were in the lowest energy bin (0.01 - 1 keV) of the DE 1/EICS summary plots. They reported that the McIlwain L value was higher, for the peak ion occurrence probability, in the local noon and dusk sectors than it was near local midnight (figure 14). Olsen *et al.* (1987) also saw this in their statistical survey. Olsen *et al.* noted that the latitudinal extent of the high probability region is local time dependant, ranging from ± 30° in the early afternoon region to ± 10° in the early dawn region.

Olsen *et al.* (1987) observed, from data collected by DE 1, that the trapped ion distribution was composed primarily of H^+, but that He^+ was seen to have a trapped component, having 10% the density of the trapped H^+, approximately 40% of the time. In one case, trapped O^+ was seen with a relative density of 0.1% that of H^+. Additionally, the trapped distribution was observed to be very localized about the equator. This is seen in the fact that the ions change from a field aligned distribution to a trapped distribution and then back very quickly as the satellite transverses the equatorial region. Figure 15 illustrates this aspect of the evolution in pitch angle distributions.

Figures 15a, 15b, and 15c show plots of flux verses pitch angle for the magnetic latitudes of -7.9°, -1.9° (approximately), and 3.6° respectively. In this case, the He^+ ions mirror the H^+ ions, although at about 3.5% of its flux. Figures 15d, 15e, and 15f show the distribution functions for H^+ in these time periods. Notice the drop in density and the increase in temperature as the satellite enters the equatorial region. (Olsen *et al.*, 1987)

Klumpar *et al.* (1987) found examples of equatorially trapped plasma in the data from the AMPTE/CCE satellite. The trapped ion distribution was found near the plasmapause interface. The temperatures of these ions were found to be on the

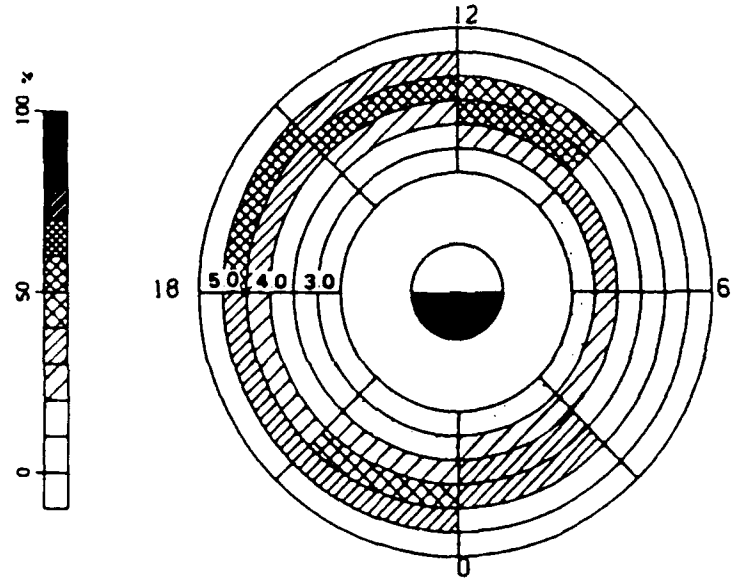

Occurrence probability of low-energy (0.01–1 keV) H^+ pancake distribution with peak ion flux above $10^5(cm^2 s\ sr)^{-1}$, within 5^c of the magnetic equator for active times ($Kp \geq 3-$) as a function of MLT and L shell. L shell bin size $\Delta L=0.5$.

Figure 14. Trapped Ion L Versus Local Time Dependence

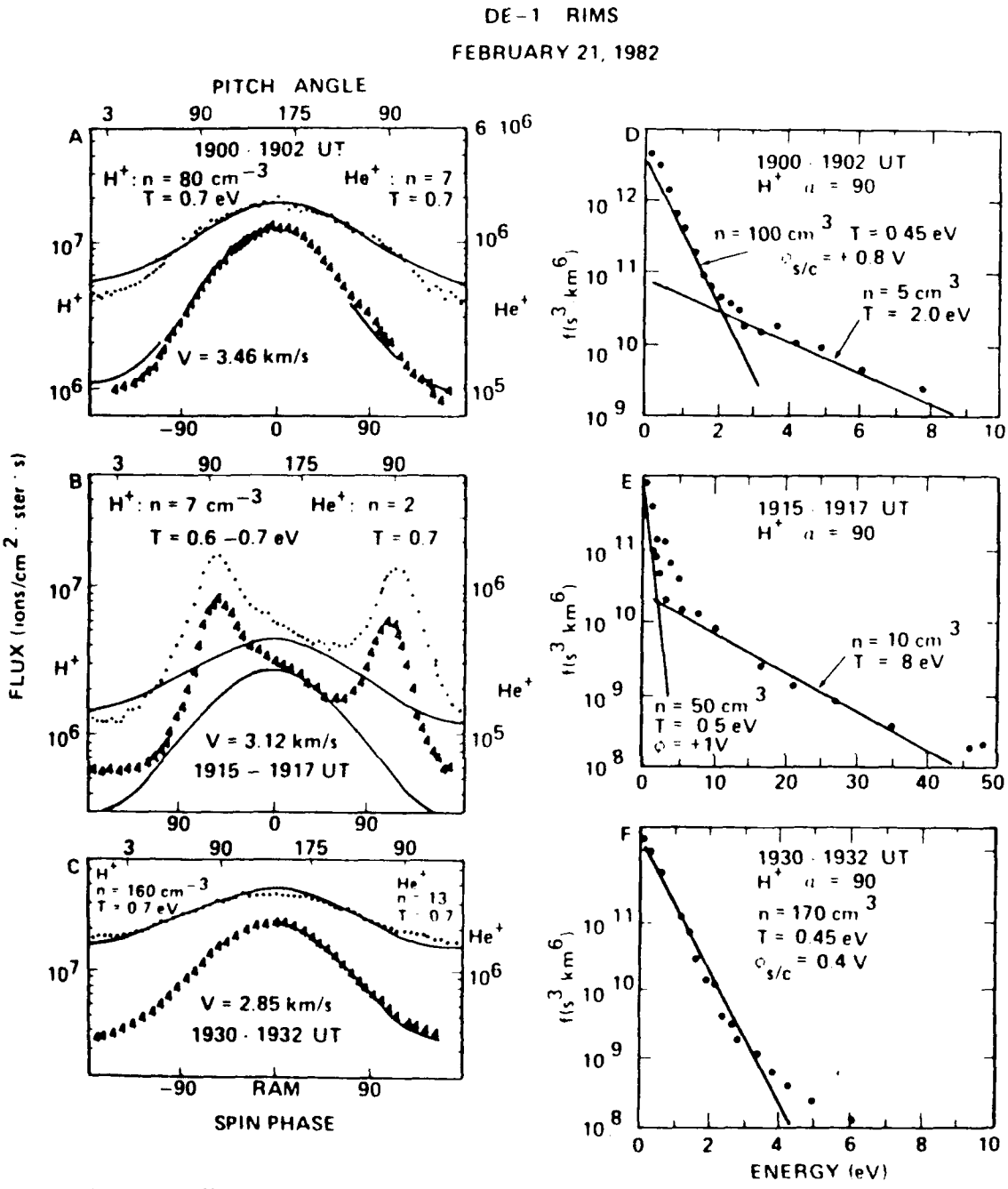

(a) Spin curves for H+ (circles) and He++ (+) superposed with fits. (b) Spin curves at the equator with lines drawn for the same temperatures found in Figures 8a and 8c at reduced densities. (c) Spin curves after the equator crossing. (d)(e)(f) distribution function for the period shown in Figure 8a. (d) H+ distribution function for the period shown in Figure 8b. Note the change in energy scale as compared to Figures 8d and 8f. (e) H+ distribution function for period shown in Figure 8c.

Figure 15. Flux - Spin Phase / Density Fits

order of 30 - 50 eV. Like Olsen (1981), they also observed that the angular distribution of the trapped ion distribution became narrower for increasing ion energies. This paper will extend this look at the AMPTE data.

There is not always a clear criteria used to define an equatorially trapped plasma. For the purpose of this paper, an equatorially trapped plasma is defined as having a specified flux in the 80° to 90° pitch angle bin (see below) in conjunction with an anisotropy greater than 1.5 (The anisotropy is defined as the ratio of the fluxes in the 80° to 90° pitch angle bin with those in the 60° to 70° pitch angle bin.) in the same time period. The survey generally was restricted to within 10° of the magnetic equator.

The minimum flux level for ions was chosen to be $10^6 (cm^2\ s\ sr)^{-1}$ while that chosen for electrons was $5 \times 10^6 (cm^2\ s\ sr)^{-1}$. These fluxes were for ions with energies centered in the 50 - 65 eV range and electrons with energies centered at 150 eV. These values were selected on the basis of previous observations and the subset of data available in the pool files.

D. THE AMPTE/CCE SATELLITE

The Active Magnetospheric Particle Tracer Explorers (AMPTE) mission consists of three satellites that were launched on August 16, 1984. The purpose of this mission was to:

> 1) investigate the transfer of mass and energy from the solar wind to the magnetosphere and to study its further transport and energization within the magnetosphere; 2) to study the interaction between artificially injected and natural space plasmas and 3) to establish the elemental and charge composition and dynamics of the charged population in the magnetosphere over a broad energy range. (Acuña *et al.*, 1985)

Two of the satellites, the Ion Release Module (IRM) and the United Kingdom Subsatellite (UKS), were concerned primarily with the introduction of artificially injected ions into the magnetosphere and will not be discussed further. The third satellite was the Charge Composition Explorer (CCE) (figure 16). The purpose of this satellite was to measure the particle distribution of the naturally occurring plasma, with respect to species, energy, and pitch angle, as well as to measure the artificially released ions from the IRM. (Dassoulas *et al.*, 1985)

The CCE was placed in an elliptical orbit around the Earth with a period of 15.66 hours and an inclination to the Earth's equatorial plane of 4.8°. It had an altitude at perigee of 1108 km and at apogee of 49,684 km (roughly 1.2 and 8.8 R_E respectively). It was spin stabilized with a spin rate of 10.25 r/min (Dassoulas *et al.*, 1985). Data began to be collected by this satellite on August 26, 1984.

The payload of the CCE (figure 17) consisted of five experiments; 1) the Hot Plasma Composition Experiment (HPCE), 2) the Charge Energy Mass Spectrometer (CHEM), 3) the Medium Energy Particle Analyzer, 4) the Magnetometer, and 5) the Plasma Wave Experiment (Dassoulas *et al.*, 1985). This paper concerns itself with data from the HPCE (and, indirectly, the Magnetometer).

E. THE HOT PLASMA COMPOSITION EXPERIMENT (HPCE)

The HPCE consists of the Ion-Mass Spectrometer and the Electron Background Environment Monitor (EBEM). The ion-mass spectrometer (figure 18) provides mass per charge ion-composition measurements from very low energies (corresponding to the spacecraft potential) to approximately 17 keV. The ions enter the detector through a collimator which limits both azimuthal and elevation angles of acceptance. The azimuthal limits are constant at ± 5.5° while the elevation acceptance angle ranges from approximately ± 25° for ions at the

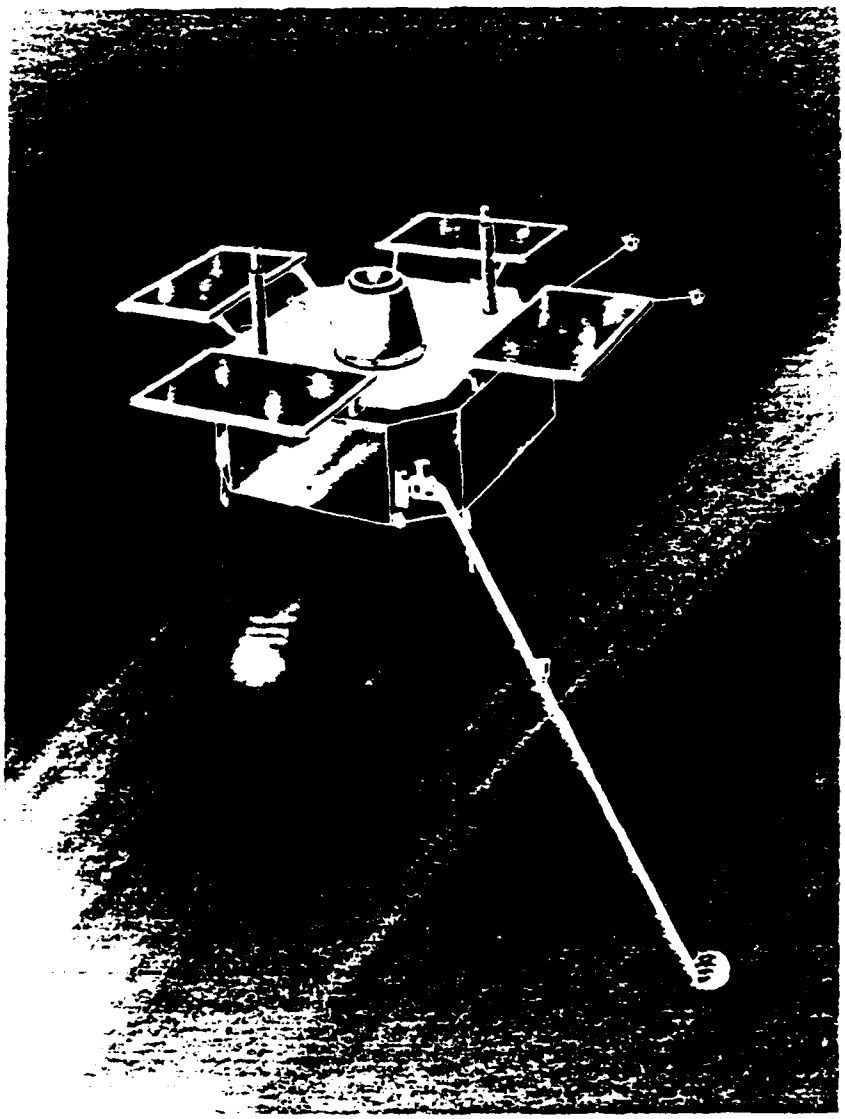

Figure 16. The AMPTE/CCE Satellite

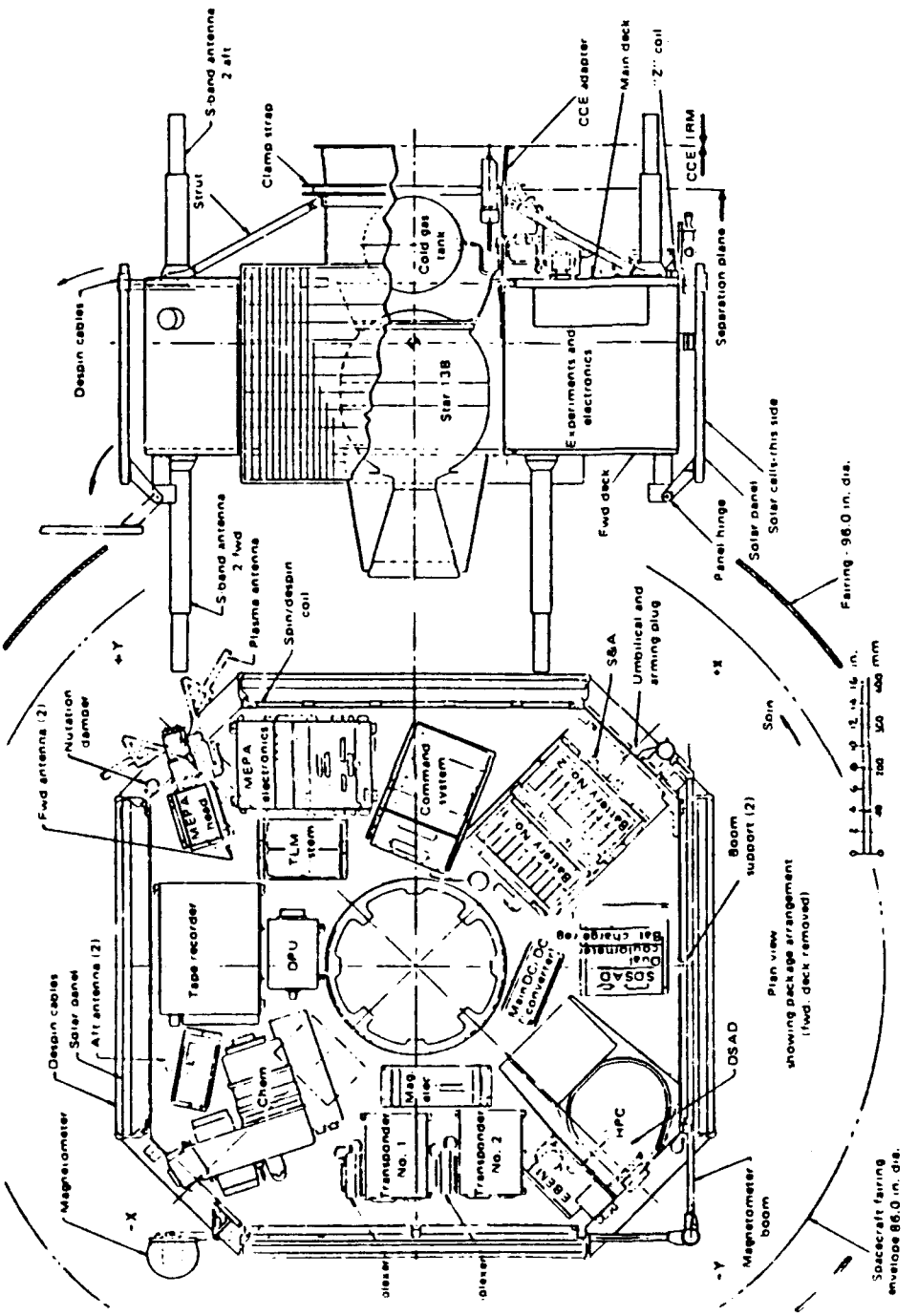

Package arrangement of the AMPTE CCE as seen from the top (left) and from the side (right).

Figure 17. The AMPTE/CCE Payload

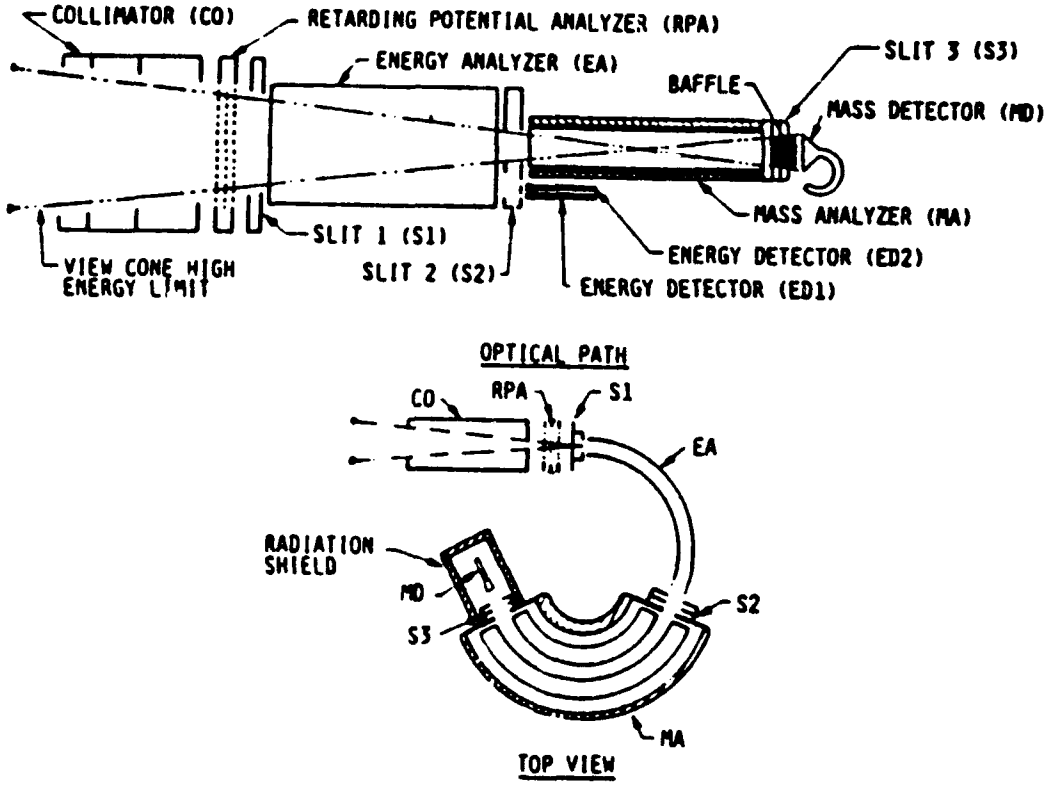

Figure 18. The HPCE Ion-Mass Spectrometer

spacecraft potential to ± 7.5° for those at 17 keV. The ions are sent through a retarding potential analyzer (RPA) and then accelerated through a -2960 V potential. (Shelley *et al.*, 1985)

The ions then pass through the object slit and into the cylindrical electrostatic energy analyzer. The electrostatic energy analyzer is programmable in 32 energy per charge steps from 3 to 20 keV/e. The central portion of the ion flux then enters the mass analyzer through a second slit, with a portion of the spectrum measured by the "energy detectors" (ED1 and ED2). The mass analyzer consists of a second cylindrical electrostatic deflection system suspended in a 978 G magnetic field. The ions that exit this region, through the image slit, are detected by a high-current electron multiplier (Shelley *et al.*, 1985). This instrument was active from August 26, 1984 until it failed on April 4, 1985.

The EBEM consisted of eight independent 180° permanent magnet electron spectrometers. Electrons entered the EBEM through a 5° full angle collimator and were then deflected through 180° by a permanent magnet (figure 19). They were then focused onto an exit aperture, that defined the allowed momentum range, and were then detected by a channel electron multiplier. (Shelley *et al.*, 1985)

Both the ion and electron data for the AMPTE/CCE HPCE were processed into pool files. These pool files consist of data arranged in 6.5 minute bins from 0000 to 2400 universal time. There is a separate data file for each day's data and each file contains both electron and ion data for that day. (Shelley *et al.*, 1985)

For this work, the ion flux measurements from the energy detectors (ED) are used, since we were not interested in differentiating between H^+ and He^+ for this survey. The pool data are sorted, by time, into 18 logarithmically spaced energy bins. The lowest four channels use the "RPA" mode data. The bulk of the data

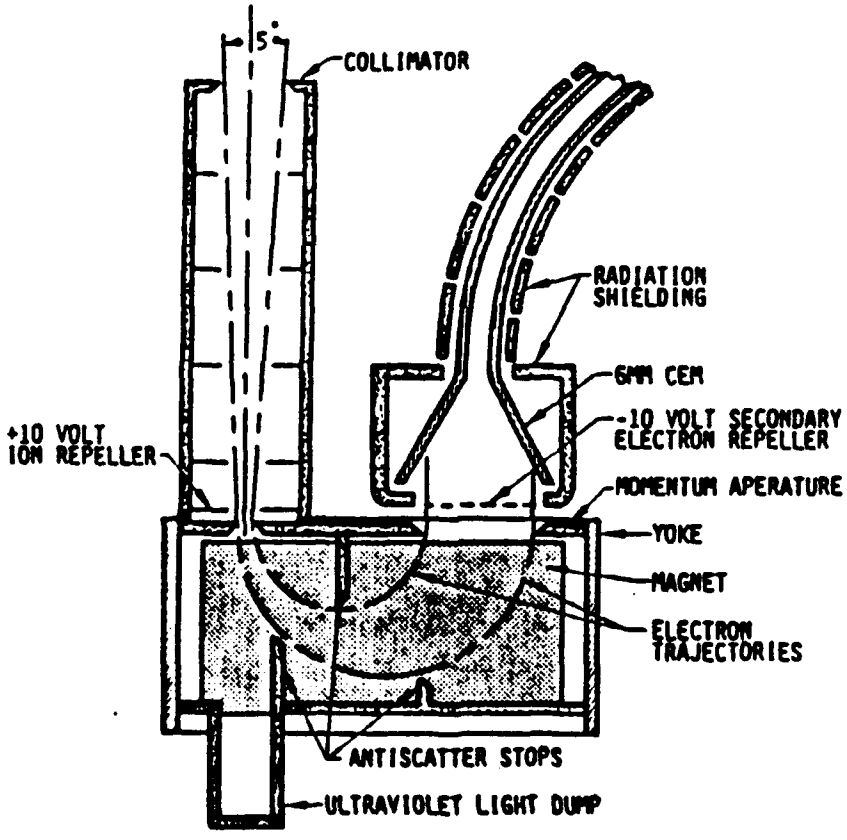

Figure 19. The HPCE Electron Background Environment Monitor

which are available in the pool file have only the fourth RPA channel, which provides an integral measurement from approximately 30 to 150 eV, with a weighted center at 50 to 65 eV. The remaining channels extend up to 17 keV/e. The ion flux is also sorted by time verses pitch angle, with pitch angle bins from 0° to 90° in increments of 10°. (Shelley *et al.*, 1985)

The electron data is likewise sorted into 8 energy bins from 50 ev to 25 keV and by pitch angle from 0° to 90° in 10° increments, each also versus time. The energy channels for the ion electrostatic energy analyzer and for the EBEM are given in TABLE 1. Data was also collected for ion species verses time verses energy and for ion species verses time verses pitch angle (Shelley *et al.*, 1985). This data was not used in this paper.

TABLE 1

ENERGY CHANNELS IN THE HPCE ON AMPTE/CCE

A. Ions

Energy Channel	Energy of Channel Center (keV/e)	Full Energy Width (keV/e)	
1	0.0014	0.0028	
2	0.0067	0.0076	
3	0.020	0.020	
4 *	0.050	0.125	RPA1
	0.052	0.122	RPA2
	0.055	0.115	RPA3
	0.065	0.095	RPA4
5	0.240	0.216	
6	0.442	0.209	
7	0.657	0.222	
8	0.885	0.235	
9	1.127	0.338	
10	1.660	0.567	
11	2.261	0.641	
12	2.941	0.724	
13	3.709	1.056	
14	5.053	1.480	
15	6.668	2.143	
16	9.339	3.041	
17	12.75	3.884	
18	17.11	2.600	

* Only one value is possible for channel 4 at a given time.

B. Electrons

Electron Detector	Energy of Channel Center (keV/e)	Full Energy Width (keV/e)
CMEA	0.067	0.051
CMEB	0.150	0.126
CMEC	0.340	0.284
CMED	0.770	0.643
CMEE	1.74	1.45
CMEF	3.94	3.28
CMEG	8.89	7.41
CMEH	20.1	11.7

III. OBSERVATIONS

A. DATA ANALYSIS

Data collected from August 26, 1984 until December 6, 1985 were processed and analyzed. However, ion data were only available through April 4, 1985. This was due to the failure of the ion-mass spectrometer on that day. The stop date for the analysis was chosen because the satellite completed one precession around the Earth, starting from August 26, 1984 and ending on December 6, 1985.

For each day of data, four spectrograms were produced. Two spectrograms presented the ion data and two the electron data. The ion spectrograms consisted of an energy channel-time spectrogram, for pitch angles in the 80° - 90° range, and a pitch angle-time spectrogram, for ions in the fourth energy channel (30 - 150 eV). The electron spectrograms consisted of an energy channel-time spectrogram, for pitch angles in the 80° - 90° range, and a pitch angle-time spectrogram, for electrons in the second energy channel (150 eV).

These spectrograms were then examined for periods when the satellite entered the magnetopause (which was evidenced by very high fluxes in all pitch angle bins as well as in most of the energy bins). The spectrograms were also inspected to find periods of very "choppy" data and periods when the instrument was undergoing diagnostic testing. Data in these periods were then removed from the data file to ensure that the analysis would not be contaminated by it.

These edited data files were then surveyed to produce probability distribution plots. These are various plots describing the probability of finding a trapped plasma using criteria which will be described below. These plots are of two basic types:

1)local time - McIlwain L plots and 2) magnetic latitude - McIlwain L plots. The results for ions and electrons were plotted separately then compared.

B. LOCAL TIME - MCILWAIN L SURVEYS

1. Ion Survey

Figure 20 shows a plot of the probability distribution for equatorially trapped ions using the lowest criteria from the previous chapter. The criteria are that the ion flux in the 80° - 90° pitch angle bin, from the fourth ion energy channel, be greater than 10^6 ions/(cm^2 s sr), that the anisotropy be greater than 1.5, and that the ions be within 10° latitude from the magnetic equator.

The grey scale for the results plot runs from 0% to 80% with zero being white and 80% being black. The coverage plot 's grey scale ranges from 0 to 200 counts and from white to black respectively. The scales are allowed to saturate (peak coverage was approximately 600 samples at apogee). Note that the 1800 to 2400 local time sector's zero occurrence probability is due to lack of coverage.

The same data for Figure 20 are alternately presented as a surface plot in Figure 21. This plot has x and y axes of local time and L. The z axis is probability of occurrence, from 0 to 100%. A contour plot is also displayed as part of this figure to facilitate the reading of the surface plot. Again, the 1800 to 2400 local time sector was not sampled.

The high probability (greater than 45%) region for these ions starts at 0500 local time at an L of 3.5. As local time increases so does the L value of the peak probability. At 1400 local time the maximum L value, 8, is reached. At that point the probability appears to drop off sharply in L as local time moves toward dusk. This, however, may be an artifact brought about by the low coverage after 1800 local time.

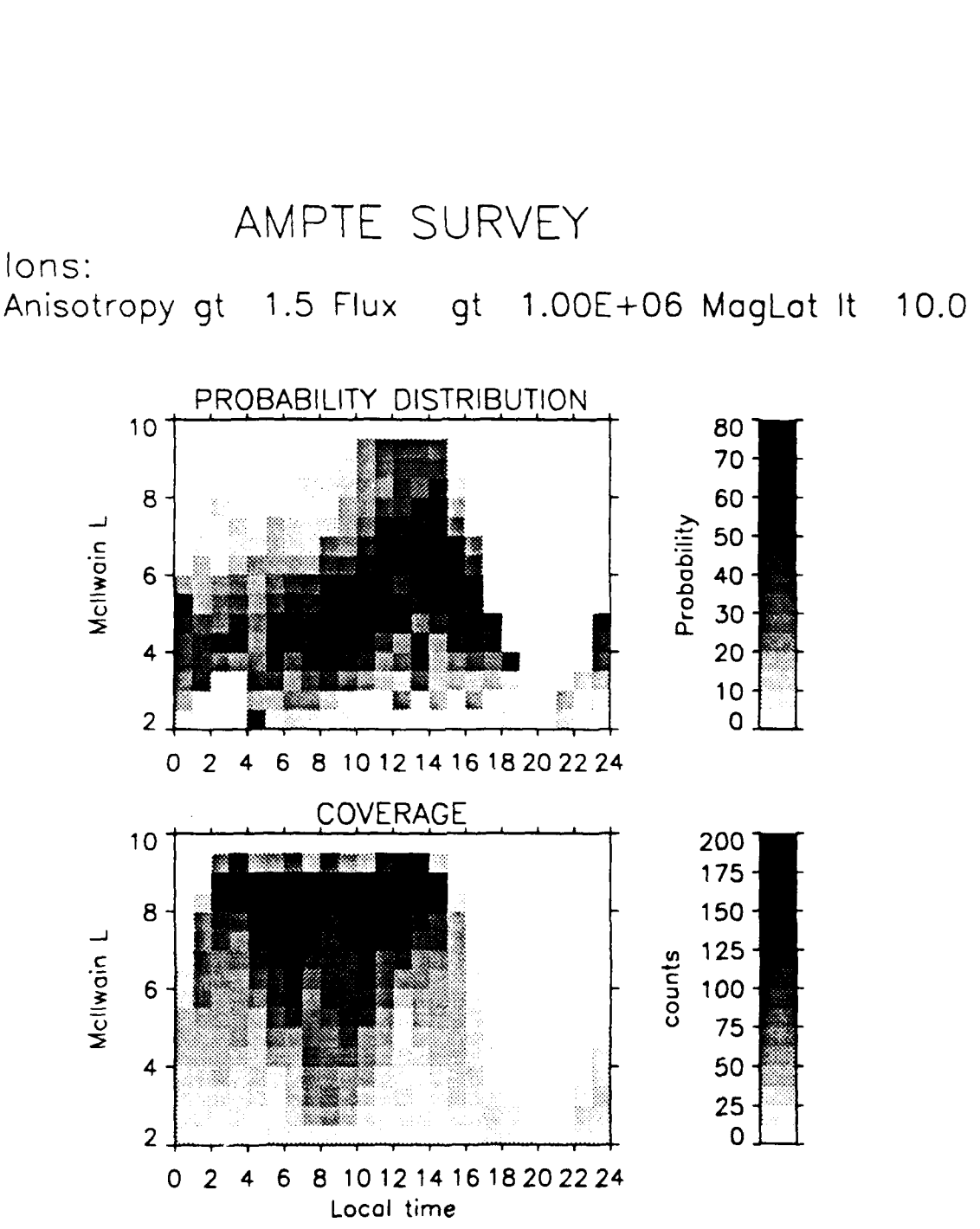

Figure 20. Trapped Ions - Flux gt 10⁶, Anisotropy gt 1.5, Maglat lt 10

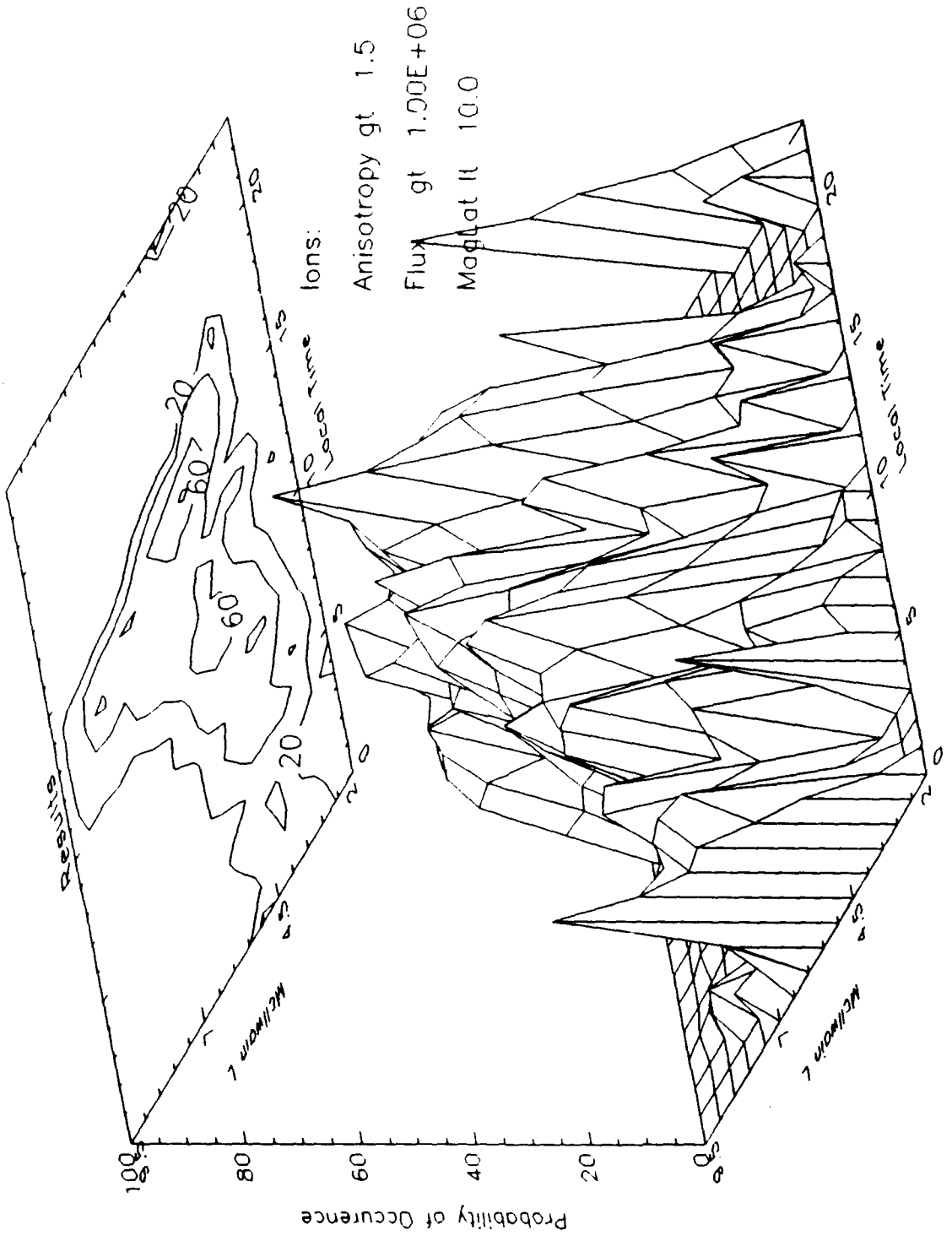

Figure 21. Trapped Ions - Flux gt 10⁶, Anisotropy gt 1.5, Maglat lt 10 - Surface Plot

In Figures 22 and 23 the results of raising the selection criteria for a trapped ion distribution are shown. In Figure 22 the selection criteria are flux greater than 5 x 10^6, anisotropy greater than 2.0, and measurements within 5° of the magnetic equator. In Figure 23 the selection criteria are flux greater than 10^7, anisotropy greater than 2.0, and measurements within 5° of the magnetic equator. The local time versus L dependence is similar in these three figures.

There is an apparent decrease in the probability of occurrence for ions in the region from 1200 to 1400 local time, most obvious in figure 23. In this region the probability drops off sharply from the expected value of 57%, or greater, to between 42% and 52%. The coverage remains high in this region, so this is probably not an artifact of the data.

2. Electron Survey

Figure 24 shows the probability distribution for trapped electrons meeting the criteria of flux greater than 5 x 10^6 electrons/(cm^2 s sr), anisotropy greater than 1.5, and for measurements within 10° of the magnetic equator in spectrogram format. Figure 25 presents this same data as a surface plot. It is readily apparent that the electron distribution is vastly different from that of the ions. There is no obvious L versus local time dependance for the electron probability distribution. In fact, the probability distribution seems to be conical in shape with the region having the highest probability being between 1000 and 1100 local time and for L values between 6 and 6.5.

The cone is not completely symmetrical however since the probability of occurrence increases to its peak value more gradually, as a function of local time, than it decreases. Changing the selection criteria does not greatly alter the shape of the distribution or the location of the peak value for occurrence probability. This can

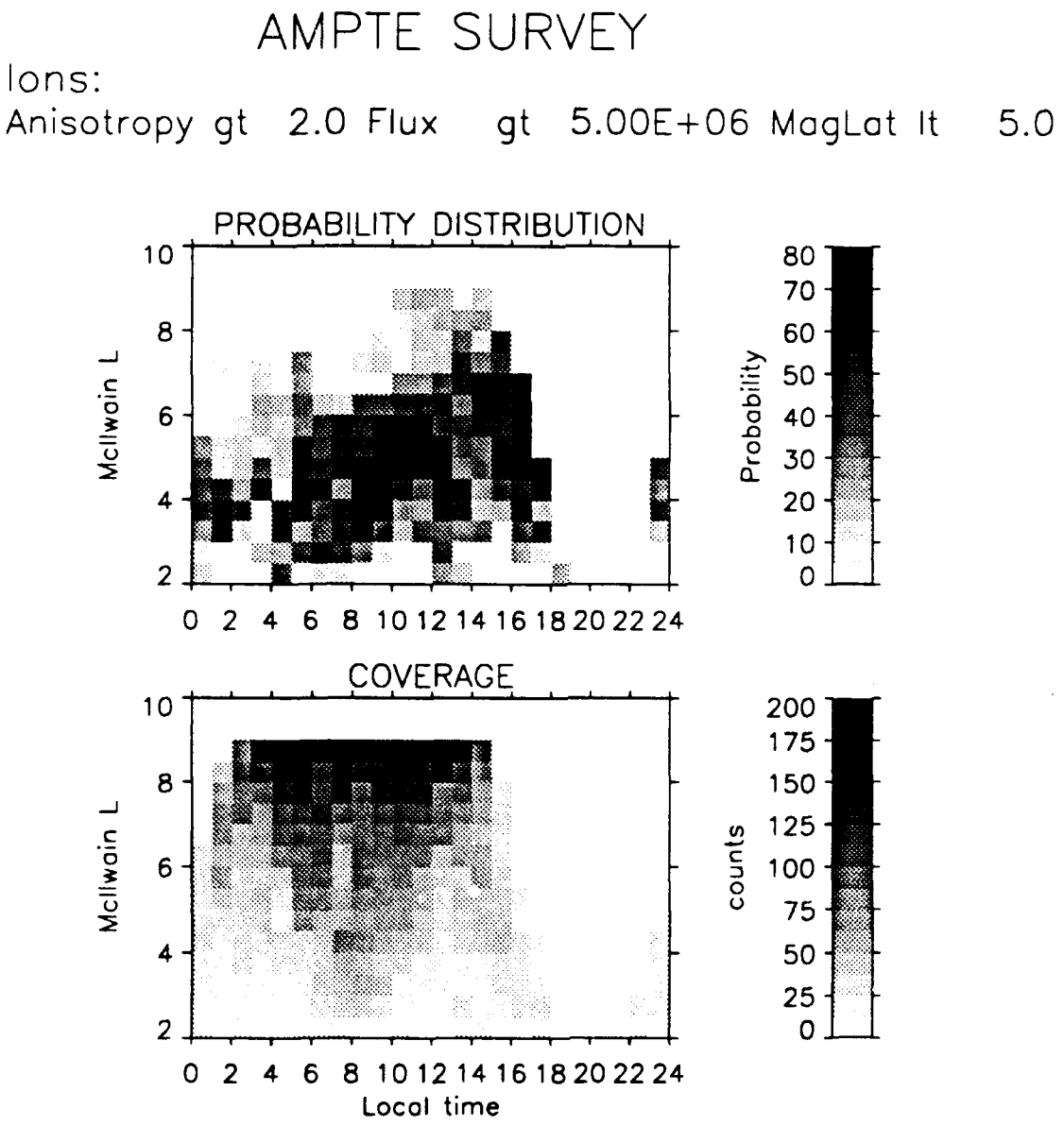

Figure 22. Trapped Ions - Flux gt 5x10⁶, Anisotropy gt 2, Maglat lt 5

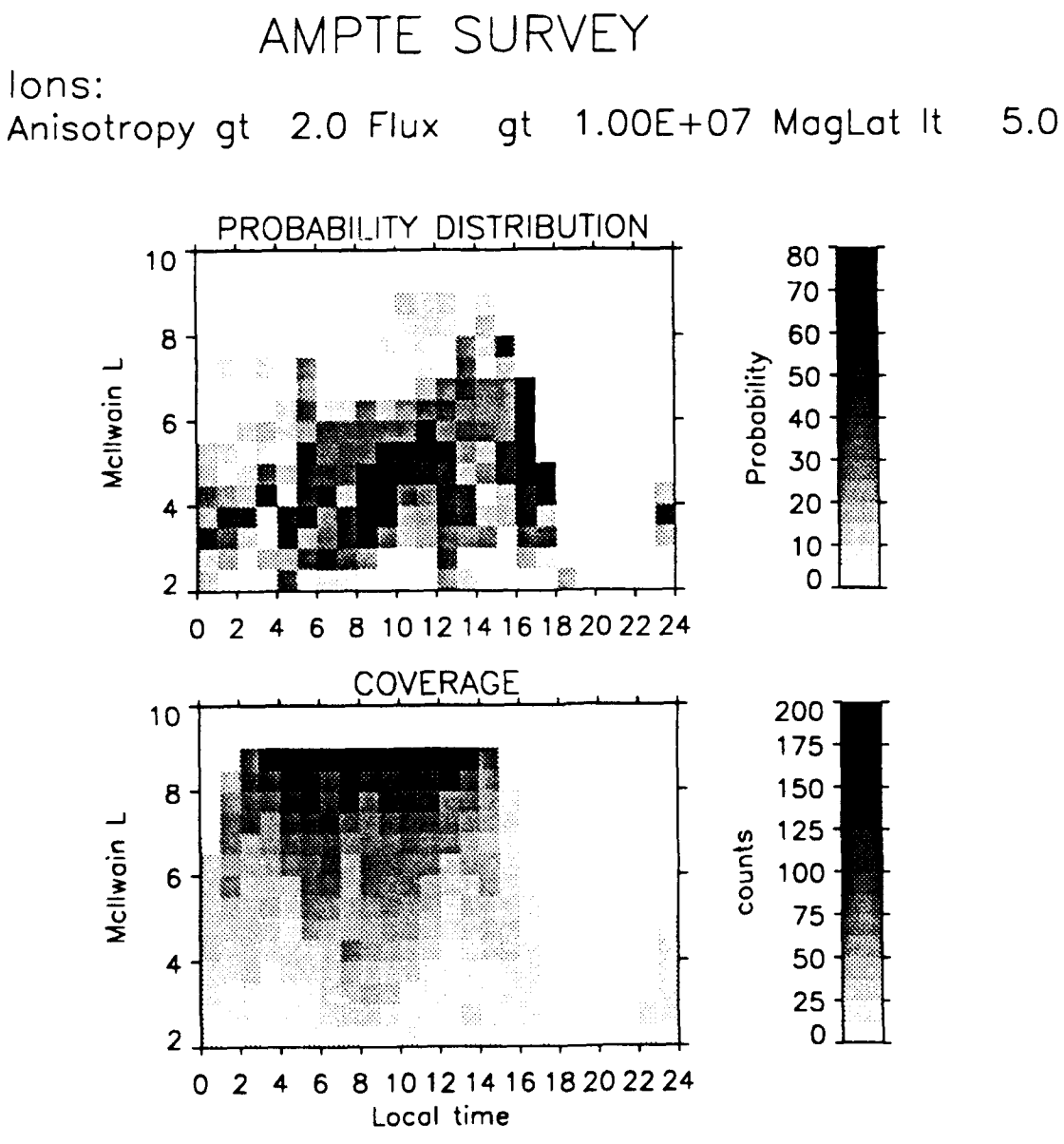

Figure 23. Trapped Ions - Flux gt 10⁷, Anisotropy gt 2, Maglat lt 5

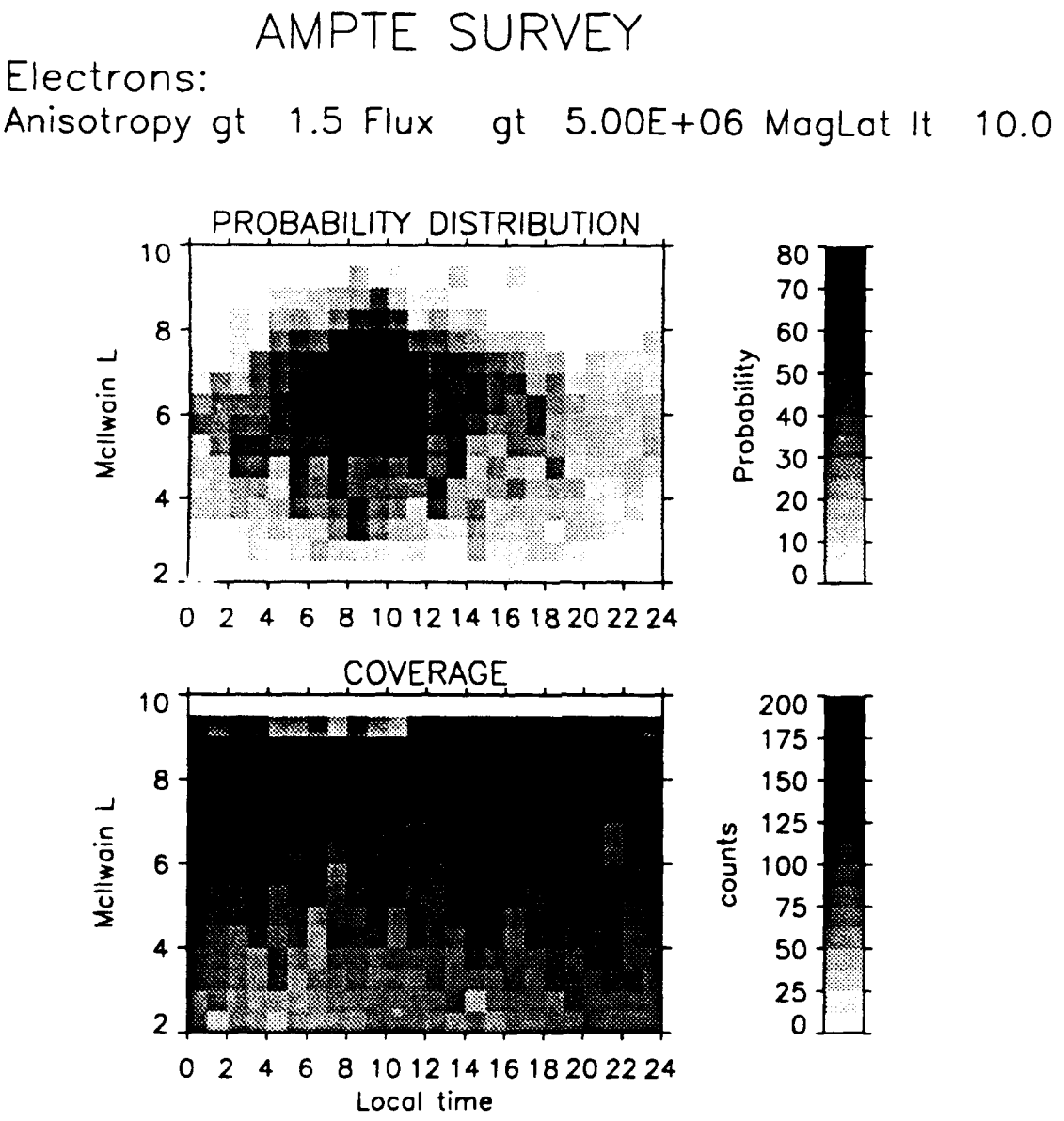

Figure 24. Trapped Electrons - Flux gt 5x10⁶, Anisotropy gt 1.5, Maglat lt 10

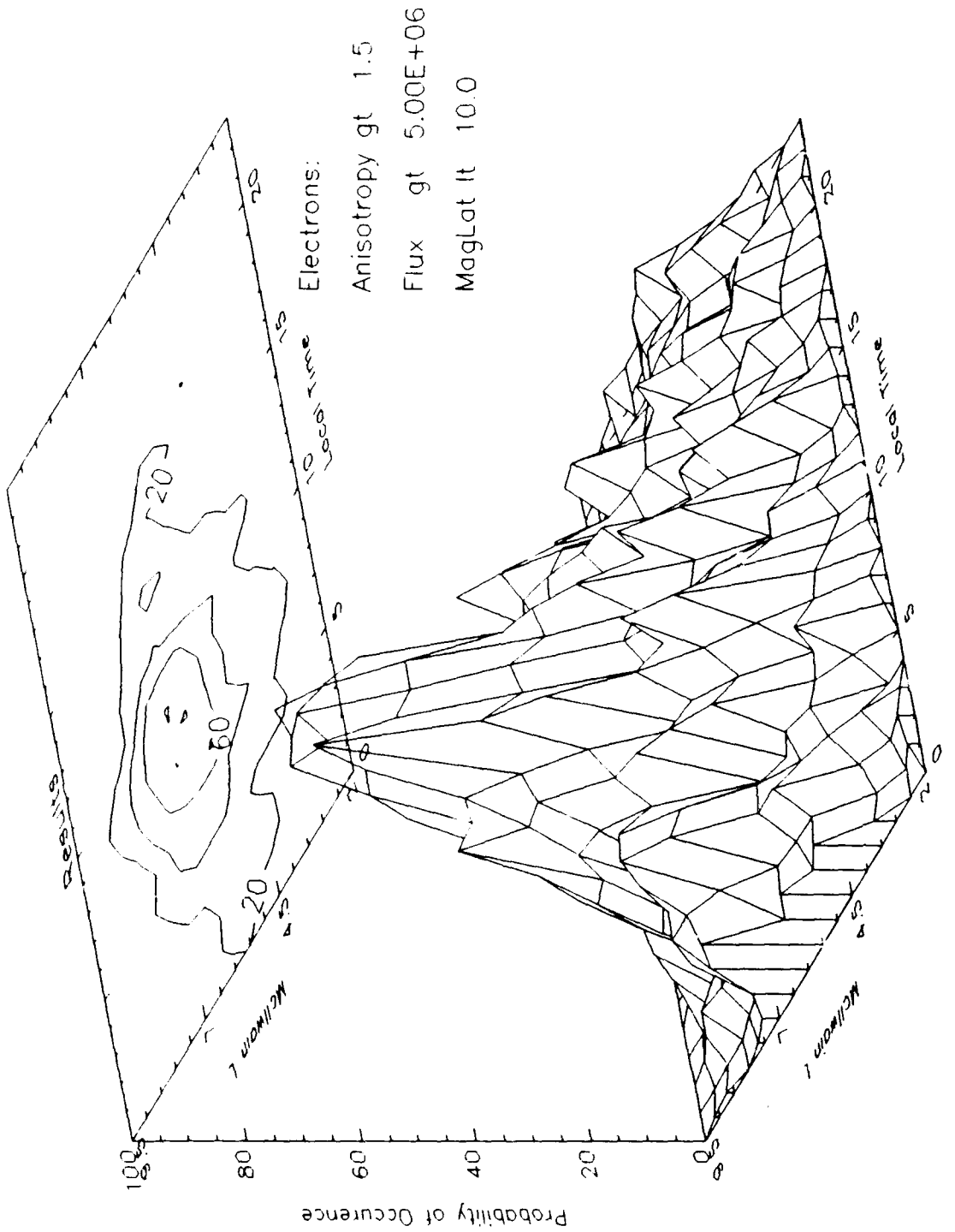

Figure 25. Trapped Electrons - Flux gt 5x10^6, Anisotropy gt 1.5, Maglat lt 10 - Surface Plot

be seen in Figures 26 and 27. Figure 26 requires fluxes greater than 5 x 10^6 and Figure 27 is for fluxes greater than 10^7. Both figures also meet the criteria of anisotropies greater than 2 and measurements within 5° of the magnetic equator. The probability of occurrence is still approximately 50% from dawn to noon for L values from 5.5 to 6.5.

C. MAGNETIC LATITUDE - MCILWAIN L SURVEY

The survey was also done in an L versus local time mode (for the regions of high probability). In the next sequence of plots, the x axis is now magnetic latitude, ranging from -10° to 10°, vice local time. The grey scale for the probability sequence was again set to range from 0 to 80%.

Figure 28 shows the location of the trapped ions with the selection criteria of flux greater than 10^6, anisotropy greater than 2, and the additional criteria that the local time for the observations be between 0800 and 1600. These times bracket the high probability region for ions and therefore allow only the region of highest probability to be sampled. The trapped ion distribution does, in fact, occur within 5° of the magnetic equator. Additionally, the average McIlwain L value is 5, which concurs with the plots presented in the previous section.

Figure 29 shows the location of the trapped electrons with the selection criteria of flux greater than 10^6, anisotropy greater than 2, and the local time range limited to 0600 to 1200. Again, the distribution is centered within 5° of the equator. However, the average McIlwain L value is much higher than the ions value. The electron distribution is centered at 6.5 L for the electrons vice 5 L for the ions.

Figures 30 and 31 show the probability distributions respectively for the ions and electrons found in the 0800 to 1200 time frame. This is the overlap region for high probability of occurrence for both trapped ion and electron distributions. The

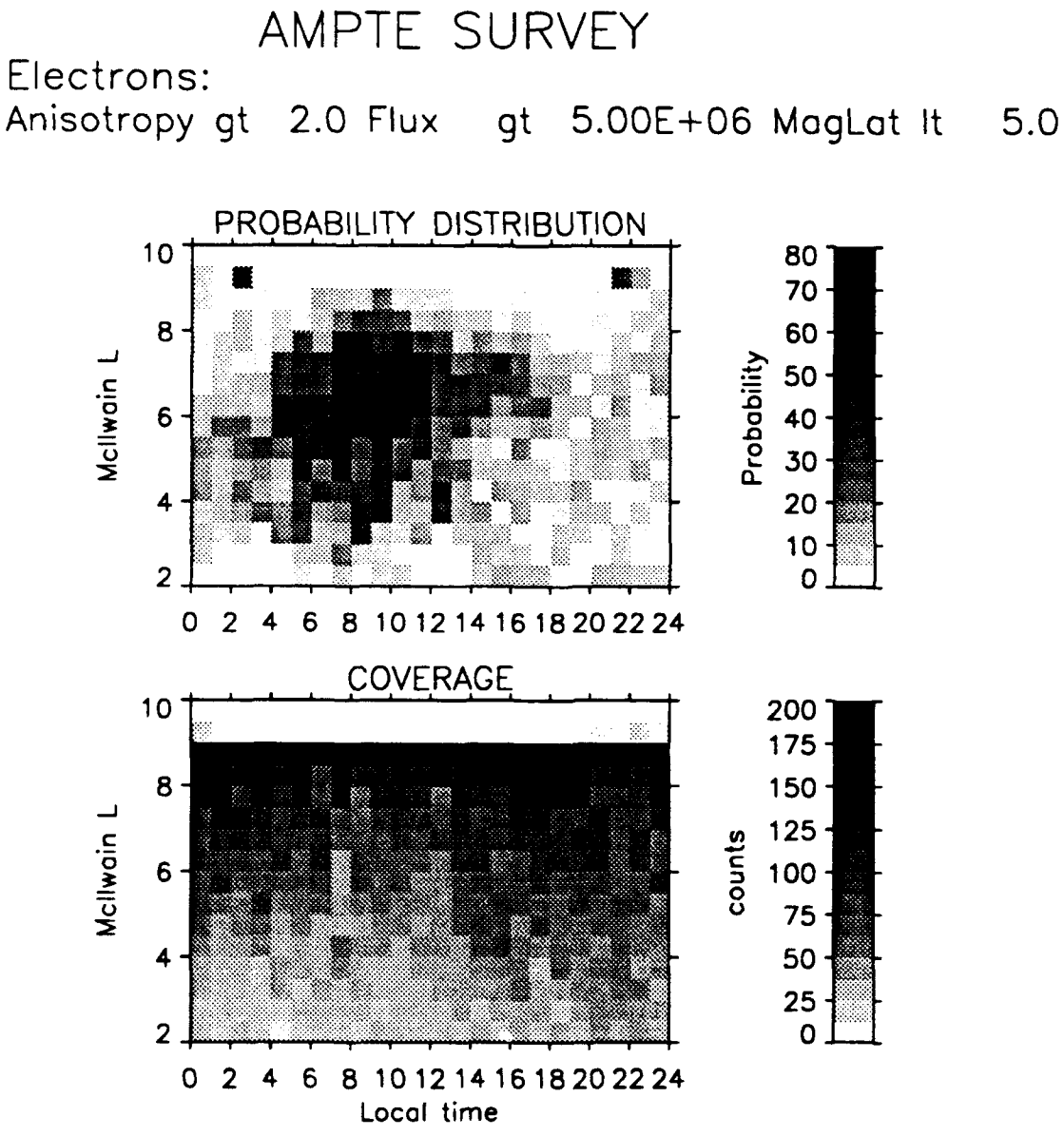

Figure 26. Trapped Electrons - Flux gt $5x10^6$, Anisotropy gt 2, Maglat lt 5

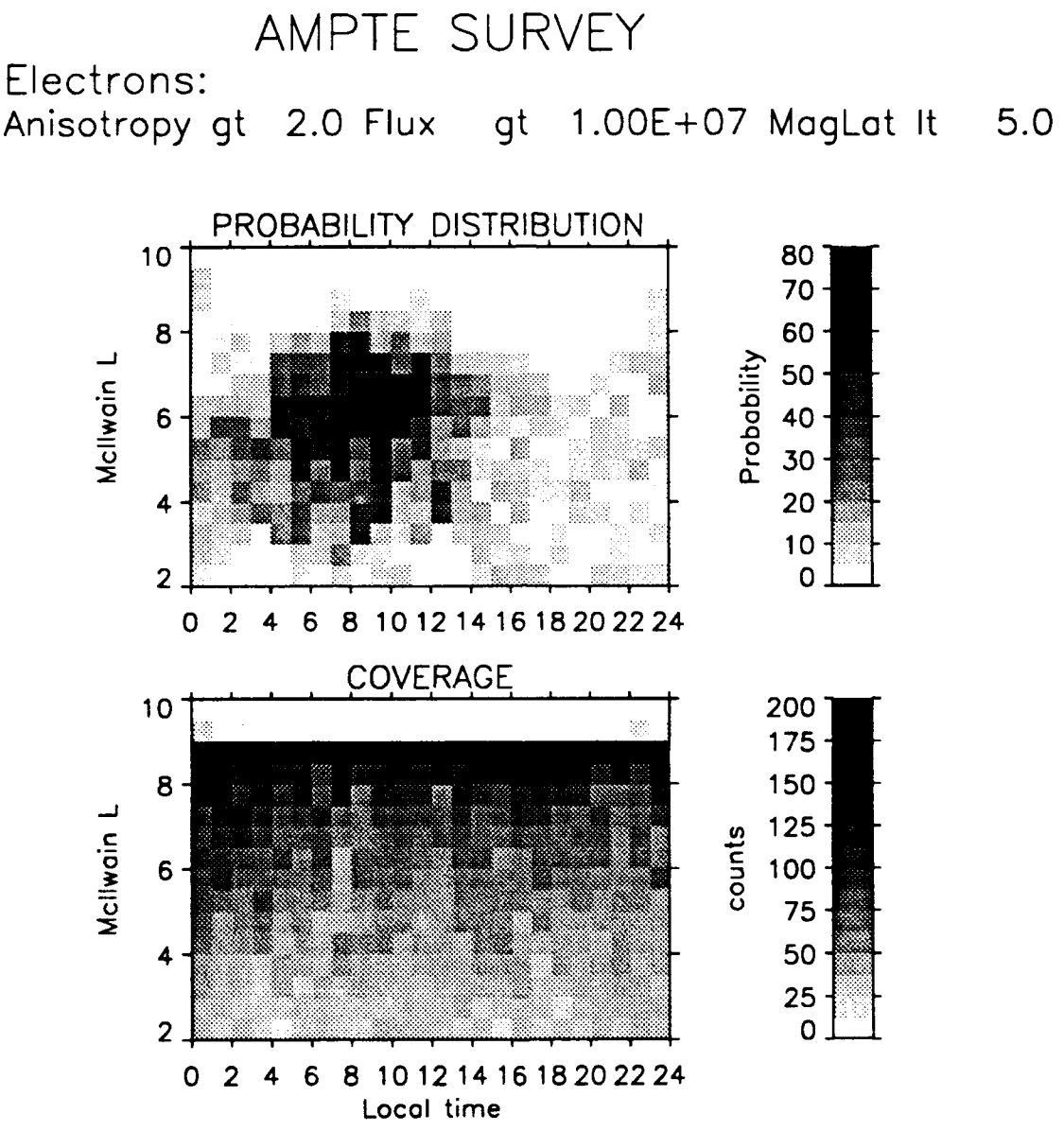

Figure 27. Trapped Electrons - Flux gt 10^7, Anisotropy gt 2, Maglat lt 5

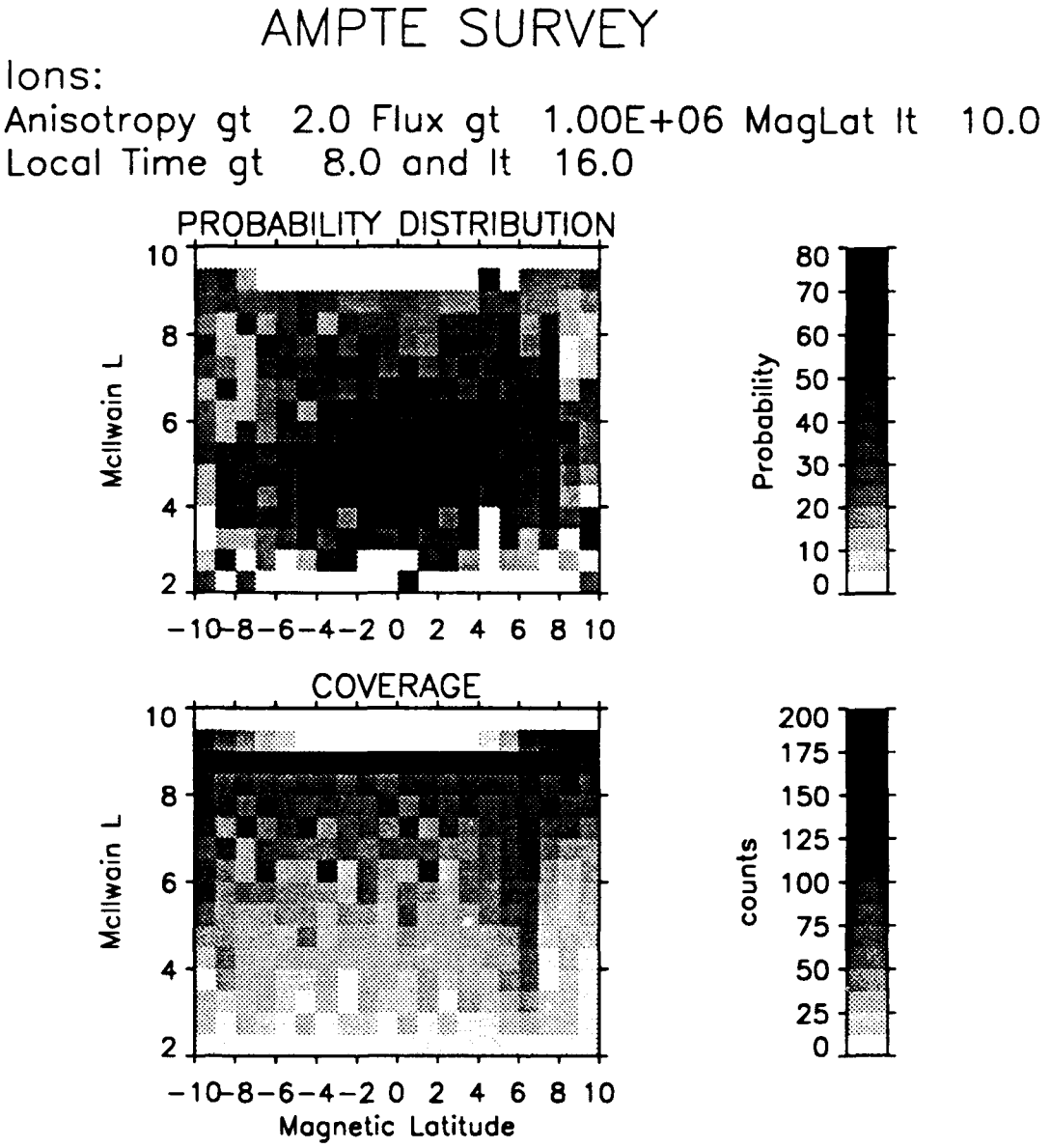

Figure 28. Trapped Ions - L vs. Maglat for Local Time 0800 - 1600

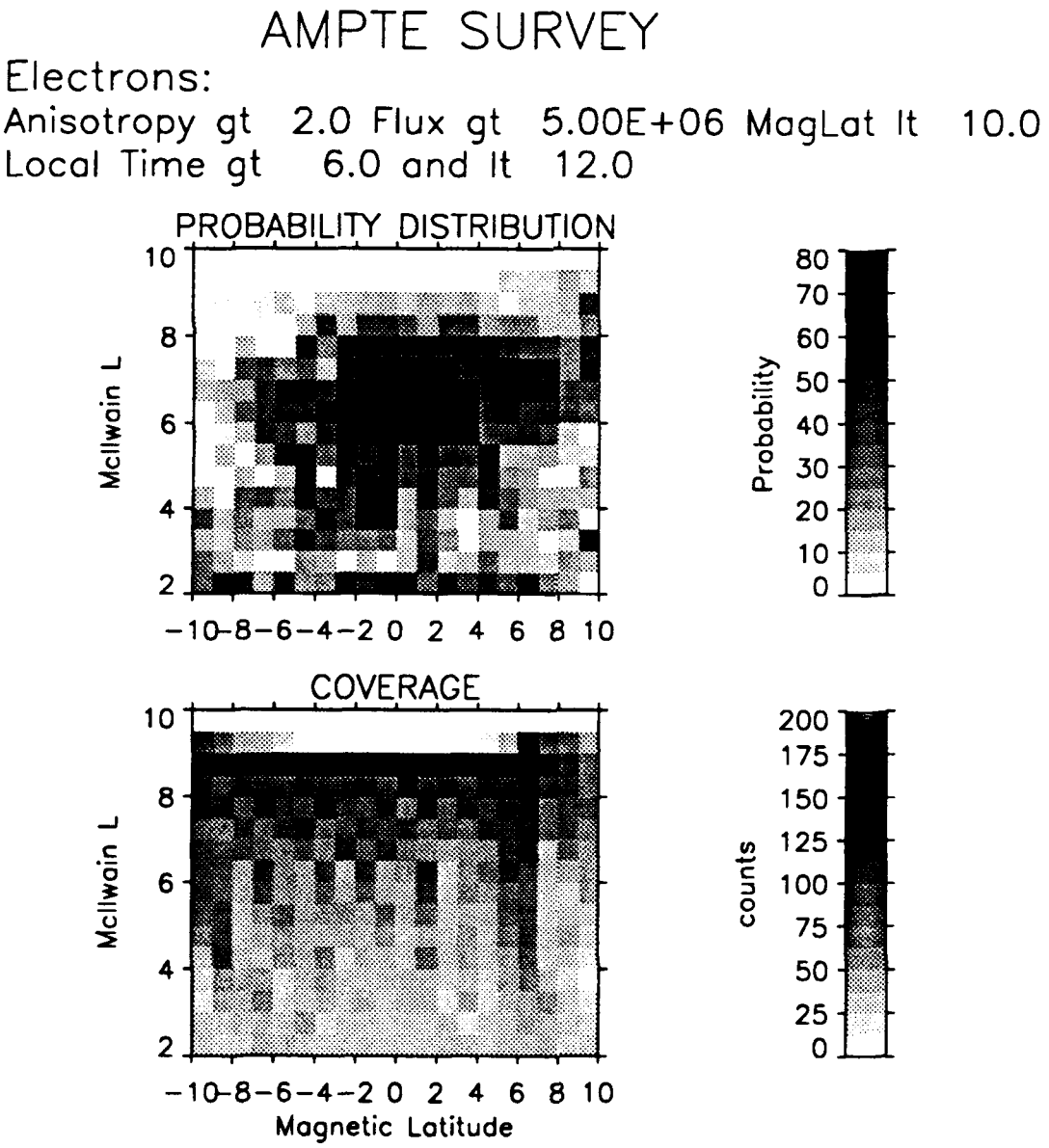

Figure 29. Trapped Electrons - L vs. Maglat for Local Time 0600 - 1200

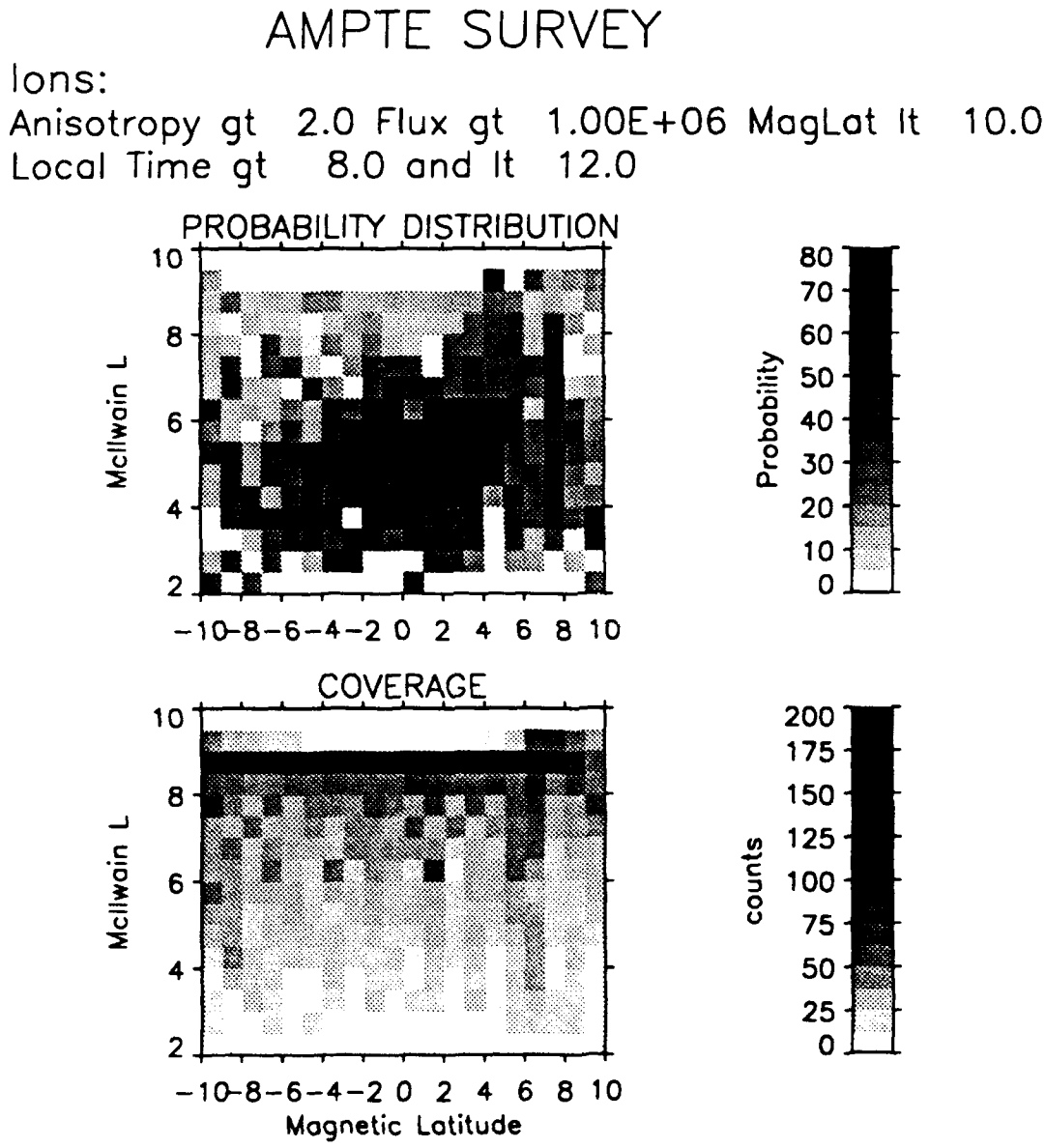

Figure 30. Trapped Ions - L vs. Maglat for Local Time 0800 - 1200

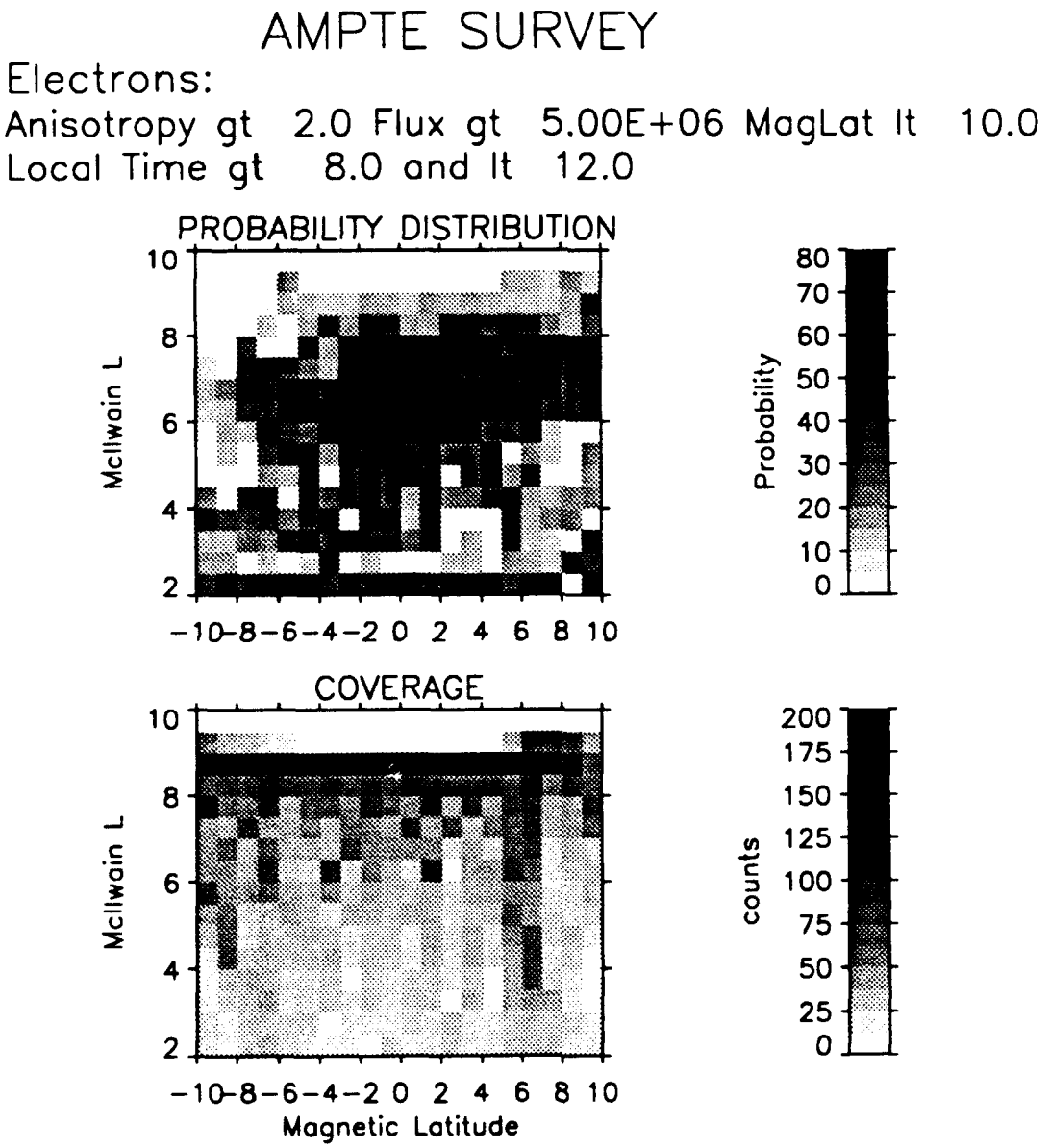

Figure 31. Trapped Electrons - L vs. Maglat for Local Time 0800 - 1200

electron probability distribution drops off sharply in the region of high ion probability. The ion distribution behaves in a complementary manner.

D. SEPARATION OF TRAPPED DISTRIBUTIONS - CASE STUDIES

The survey results indicate a separation between the high probability regions for the trapped ions and electrons. This separation can also be seen during individual orbit sequences. For plasma distributions meeting the selection criteria put forth earlier, trapped ions are seen usually at lower altitudes than trapped electrons.

TABLE 2 is a listing of the "large" event trapped plasma distributions. These observation periods showed ions and electrons with fluxes in the 80° - 90° pitch angle bin greater than 10^7 particles/(cm^2 s sr), anisotropies greater than 2, and measurements within 5° of the magnetic equator (These trapped ion and electron distributions occur on the same leg of the same orbit). The McIlwain L value at the location of the peak flux for each specie is listed. The data in TABLE 2 are presented graphically in Figure 32.

For the 55 events that fit the above criteria, 45 of the trapped ion distributions peak at a lower L value than that of their related trapped electron distributions. Additionally, there were another 4 that peaked at the same L value. The data of day 84315 (November 10, 1984) illustrates this separation.

Figure 33 shows the satellite's orbit data for day 84315 as a function of universal time. The top panel shows the satellite's altitude in terms of the McIlwain L parameter, the middle panel shows its magnetic latitude, and the bottom panel shows where the satellite is with respect to local time.

Taking the location of the plasmapause to be at approximately L = 4.5, it can be seen that there will be four crossings of this boundary on day 84315. An overview of the ion and electron fluxes, in the 80° - 90° pitch angle bin, for the

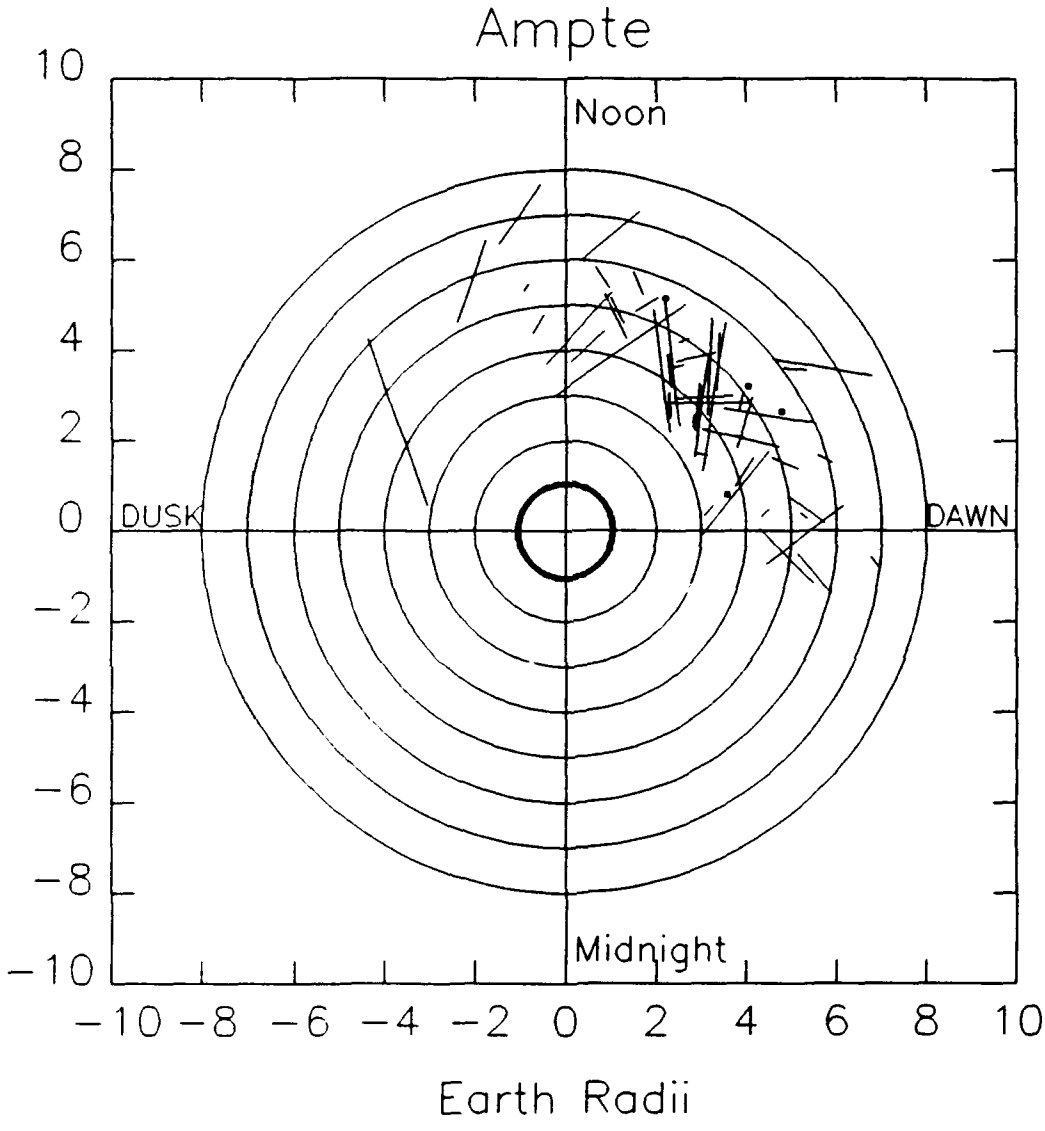

Figure 32. Separation of Large Ion and Electron Events

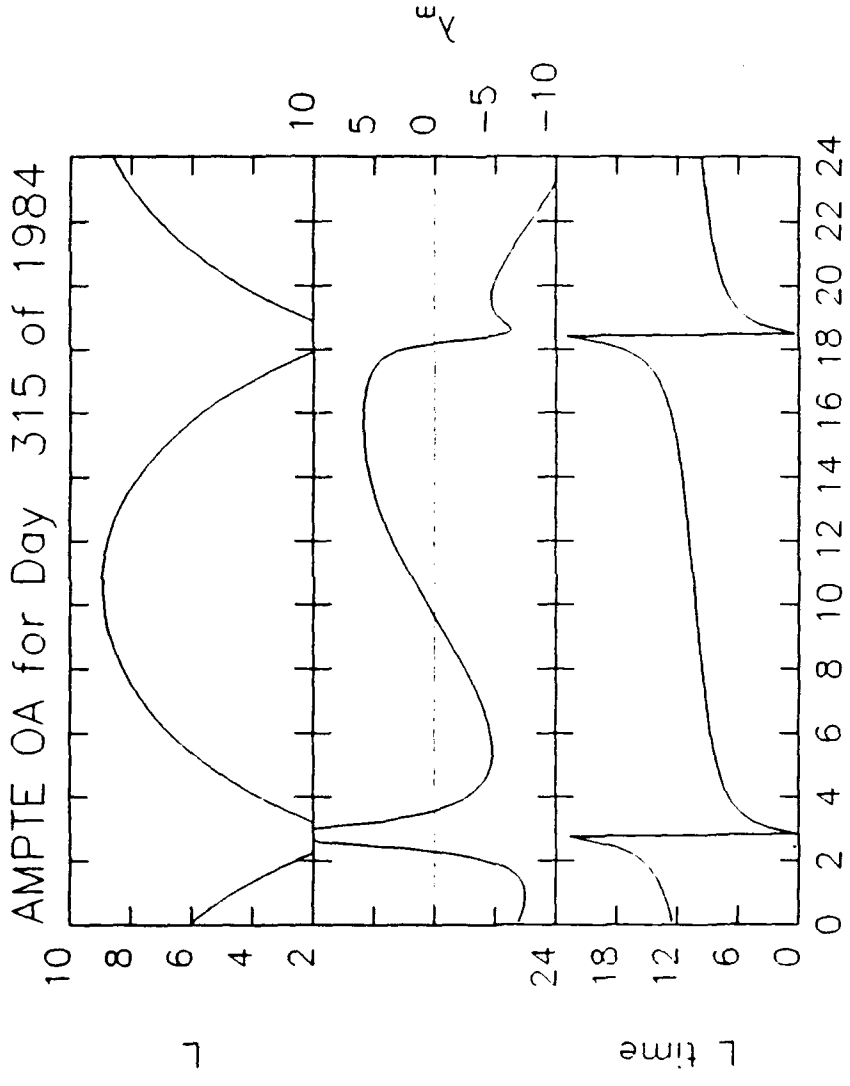

Figure 33. Orbit Data Day 84315

entire day of 84315 is shown in Figure 34. The anisotropies are shown in the bottom half of Figure 34. Plus signs represent ion data and the solid line represents electron data in this figure.

The first two of the boundary crossings occur at approximately 0105 and 0425 universal time respectively. The ion and electron fluxes for these crossings are shown in more detail in Figure 35. For the first of these crossings there is a noticeable separation in when, and therefore where, the peak flux occurs. The electron flux peaks at 0019 UT which corresponds to a local time of 1247 and an L value of 5.67. The ion peak occurs at 0058 UT (1324 local time and L = 4.7). The anisotropies for both the ions and electrons are over 2 for these times.

At the second crossing, the ions and electrons peak at the same time. This occurs at 0357 UT, 0652 local time, and L = 3.67. Again the ion and electron anisotropies are greater than 2 at this time. Note the relative reversal in the anisotropies. At approximately 0100, the ion anisotropy exceeds that for the electrons. The converse is true at 0400. This effect depends on the energies surveyed. The ion anisotropy at 50 eV is generally higher for trapped distributions than the electron anisotropy at 150 eV.

Data for the third and fourth crossings of the plasmapause are shown in Figure 36. The third crossing will not be considered since the plasma does not meet the criteria of a trapped distribution. This is due to the low anisotropies for both the ions and electrons for this crossing.

The fourth crossing again shows a separation in the ion and electron peak. The ion flux peak occurs at 1944 UT, 0659 local time, and L = 3.87. The electron flux, on the other hand, peaks at 2016 UT, 0740 local time, and L = 4.82. The ion anisotropy is 2.17 at the time of maximum flux and the electron's anisotropy is 1.59

at the time of their peak flux. Therefore, both meet the criteria for a trapped distribution.

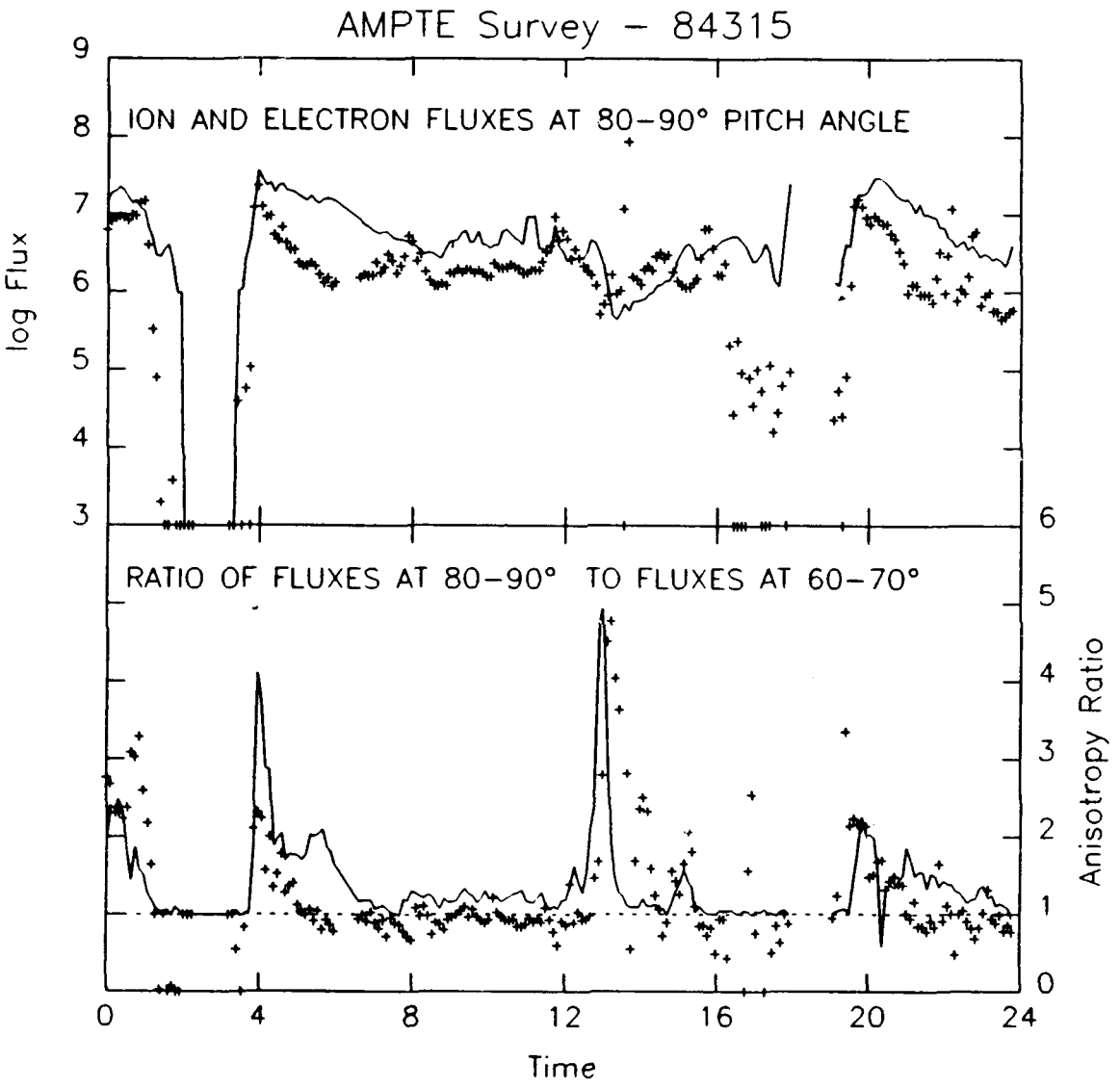

Figure 34. Day 84315 - Pitch Angle Dist. and Anisotropies

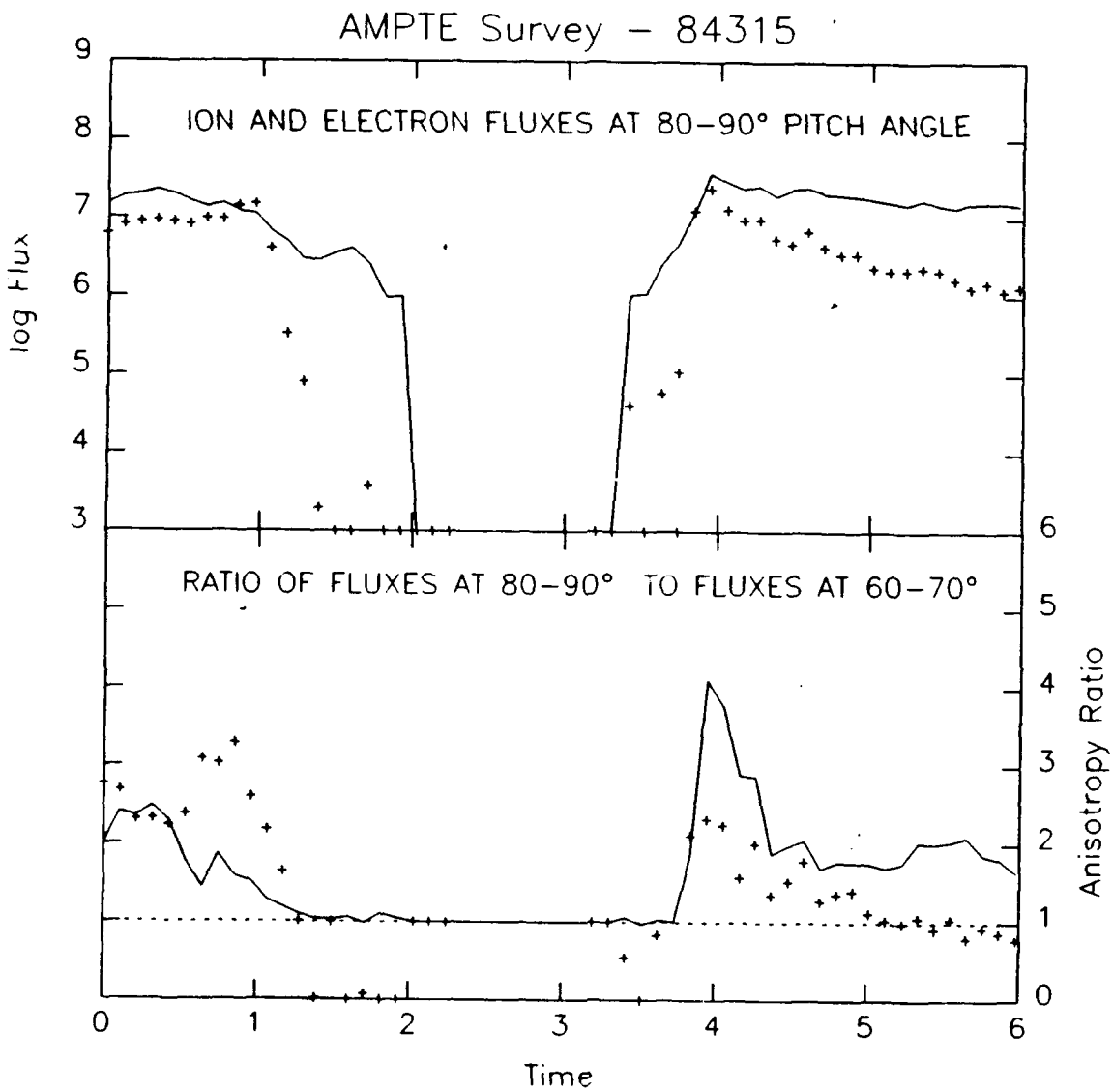

Figure 35. Day 84315, 0000-0600 LT, - Pitch Angle Dist. and Anisotropies

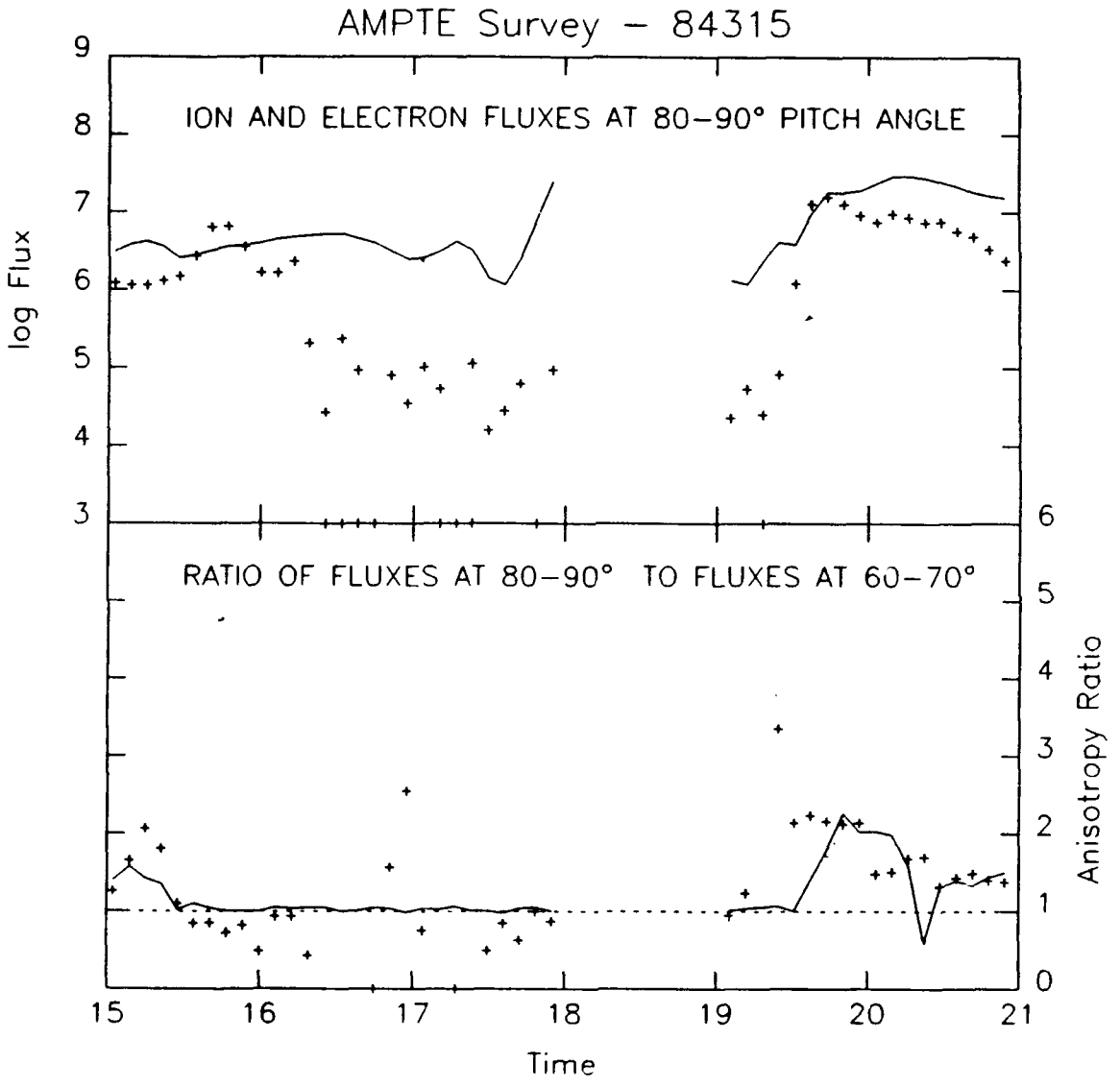

Figure 36. Day 84315, 1500-2100 LT, - Pitch Angle Dist. and Anisotropies

TABLE 2

LOCATIONS OF "LARGE" EVENTS

	Electron Peak Flux		Ion Peak Flux	
Day	Local Time	McIlwain L	Local Time	McIlwain L
84245	1122	5.31	1050	4.46
84247	1058	4.76	1116	5.26
84251	1134	5.87	1119	5.44
84262	1102	5.92	1047	5.49
84264	0933	3.83	0909	3.41
84264	1034	5.27	0854	3.17
84266	1503	6.09	1719	3.11
84266	1000	4.52	0934	3.95
84270	1028	5.58	0852	3.42
84281	0837	3.64	0849	3.85
84281	0910	4.43	0832	3.63
84283	0907	4.38	0837	3.78
84283	0844	3.97	0823	3.55
84285	0923	5.00	0800	3.27
84287	0943	5.73	0837	4.07
84294	0929	5.57	0851	4.59
84296	0930	5.81	0735	3.30
84302	0819	4.67	0832	5.01
84303	1216	7.71	1252	6.52
84304	1301	6.68	1350	5.18
84309	0833	5.18	0833	5.18
84311	0822	5.11	0744	4.22
84313	0641	3.31	0625	3.08
84315	0652	3.67	0652	3.67
84315	0726	4.46	0659	3.87
84318	1234	5.53	1240	5.38
84319	0756	5.49	0756	5.49
84321	0726	4.83	0554	3.02
84336	1108	7.26	1146	6.00
84336	0625	4.53	0617	4.35

TABLE 2 (cont.)

Day	Electron Peak		Ion Peak	
84338	1223	4.82	1238	4.45
84351	1116	5.37	1227	3.72
84352	1116	4.51	1153	3.73
84354	1034	5.55	1050	5.08
84355	0621	6.17	0523	4.51
84358	1027	5.61	1027	5.61
85002	1009	5.65	1216	3.01
85009	0950	5.04	0956	4.87
85018	0747	7.63	0838	5.97
85021	0920	5.17	0948	4.48
85022	0815	6.42	0827	6.04
85023	0938	4.52	0947	4.34
85038	0835	4.78	0920	3.83
85039	0734	6.01	0831	4.44
85040	0818	5.00	0922	3.68
85052	0758	4.27	0750	4.46
85053	0707	5.81	0658	6.09
85055	0726	5.08	0827	3.77
85058	0701	5.34	0719	4.84
85067	0753	3.55	0805	3.33
85070	0540	6.78	0533	7.00
85072	0607	5.75	0635	5.02
85073	0612	5.37	0618	5.22
85089	0507	6.04	0538	5.15
85090	0511	5.63	0604	4.30

IV. DISCUSSION

The probability distributions for equatorially trapped ions and electrons show a clear localization for regions of high occurrence probability ($\geq$ 50%). This is particularly true for the electrons. The electron distribution has a very localized peak at 0900 local time, L = 6, and within 5° of the magnetic equator. This is seen regardless of selection criteria used in the surveys.

The trapped ion distributions differ from those published previously, in some aspects. The local-time versus L plots presented in Figures 20 through 23 differ, for example, with those shown by Sagawa *et al.* (1987). The DE 1/EICS survey of low energy (0.01 - 1 keV) H^+ ions shows an increase in L for the peak occurrence probability with a maximum value in the dusk region (reshown as Figure 37a). Results shown here (figure 20) give a maximum at 1400 local time.

This disagreement may have a number of causes. Foremost are an inadequate number of samples for the dusk region in this survey. It is likely that if the AMPTE/HPCE data extended into the dusk region, we would have found even higher occurrence probabilities. Also, the data shown in Figure 37a are only for active times (Kp $\geq$ 3-), whereas the survey results given here are for all magnetic activity levels.

Sagawa *et al.* (1987) do not show a decrease in probability for the region from 1200 to 1500 local time. Figure 37 compares data from the AMPTE/CCE satellite with Sagawa *et al.*'s survey plot. Sagawa *et al.*'s survey plot (figure 37a) shows a monotonic increase in probability with local time, peaking at 1800. The AMPTE/CCE survey (figure 37b), replotted on the same scale to facilitate

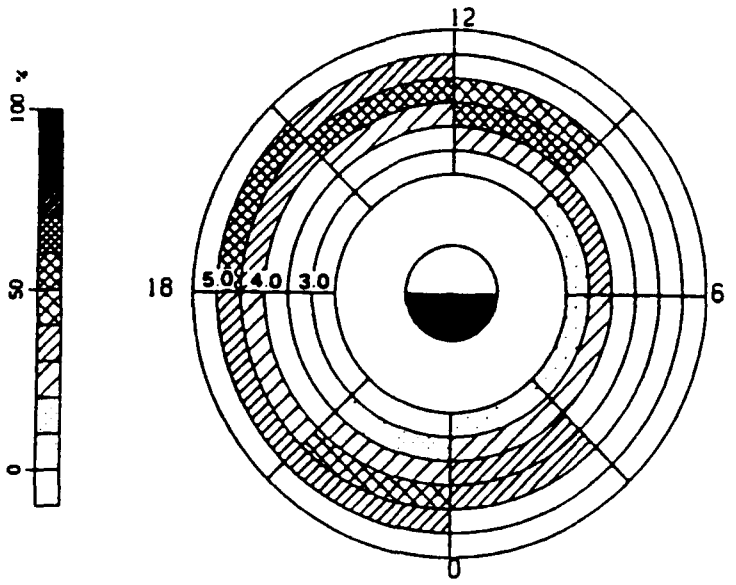

a.

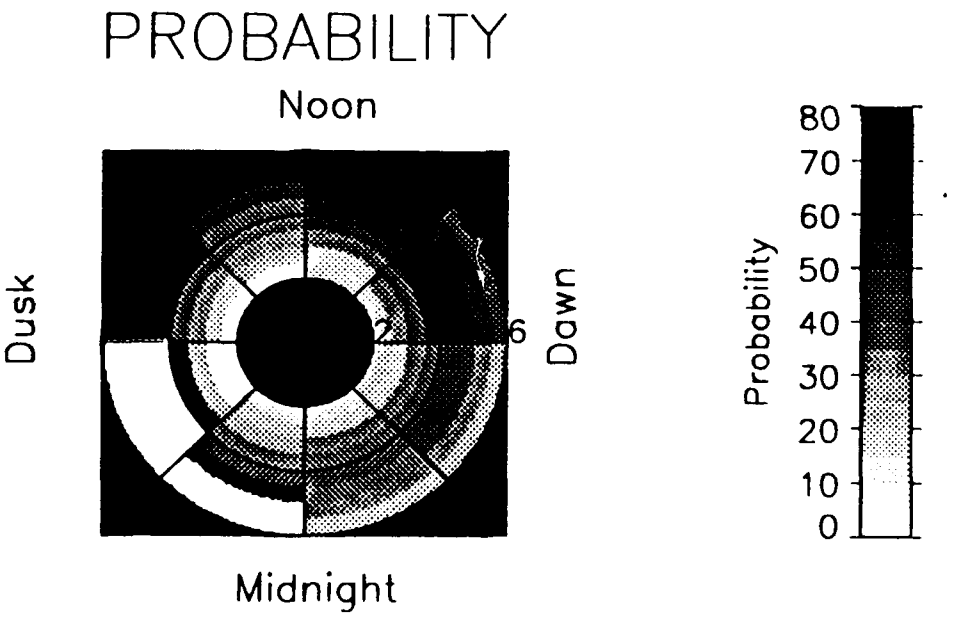

b.

Figure 37. Comparison of Occurrence Probability Plots

comparison, clearly shows a substantial decrease in occurrence probability in the 1200 to 1500 local time sector.

We suspect this difference is due to the difference in energy ranges used for the two surveys. Sagawa *et al.* used summary results from approximately 10 eV to 1 keV, whereas this work used approximately 50 to 150 eV ion measurements. Therefore, the survey done for this thesis may not accurately reflect the total trapped ion distribution.

Olsen *et al.* (1987) did see this feature in their statistical survey of 0 to 100 eV H^+ ions. Plate 7a from that paper shows a region of decreased probability from 1200 to 1300 local time and for L between 3 and 5. The region from 1300 to 1400 and L from 3.5 to 4.5 may also show this decrease. This lends credence to the idea that this low probability region is not an artifact in the survey. The likeliest explanation is that the average energy of the equatorially trapped ions goes above 150 eV, in this local time region.

The shape of the probability distributions presented in figures 20 through 23 show a structure which can be explained in terms of the plasmapause location. Figure 38 is taken from Williams *et al.* (1981). It shows the location of the plasmapause as a function of local time. The shape of this plot mimics the shape of the ion 58% probability distribution contour from Figure 21. The distribution shown there is replotted here in Figure 39 as a contour plot. The similarity in shapes suggests an interrelation between the location of the plasmapause and the location of the trapped ions.

This concurs with Horwitz *et al.* (1981) who observed that trapped ion distributions tended to occur along the plasmapause boundary in the dawn to dusk

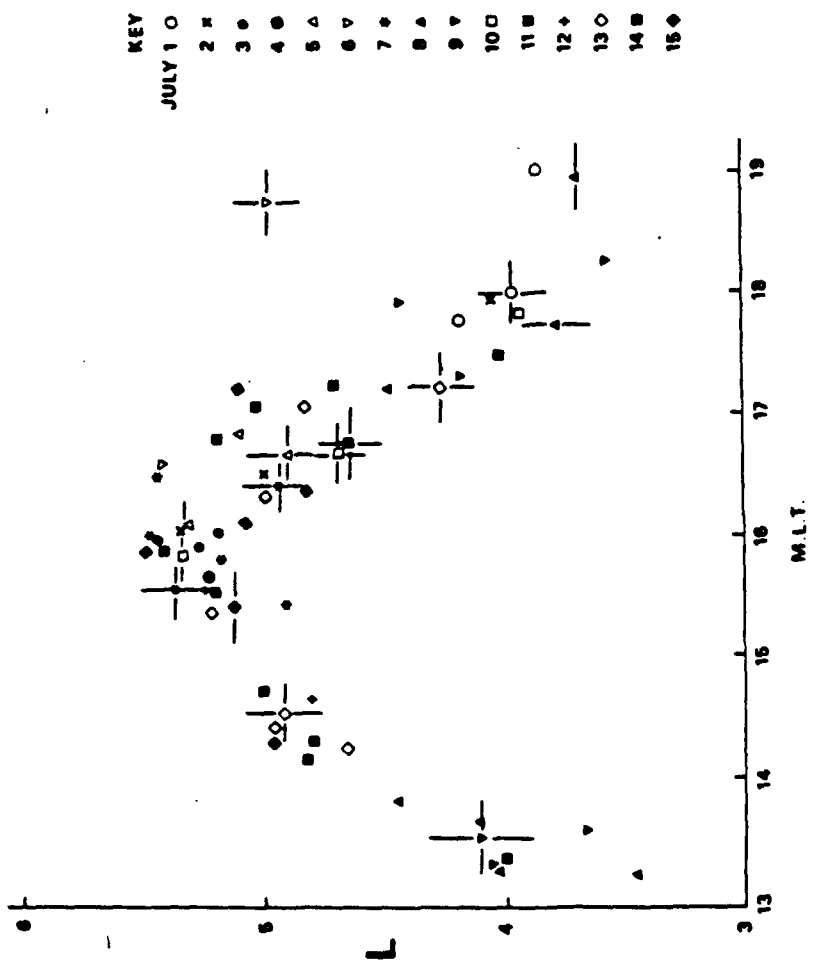

L-value of plasmapause, on different days in July 1972, derived from Explorer 45 (S^3-A) data and plotted against magnetic local time.

Figure 38. Plasmapause Location

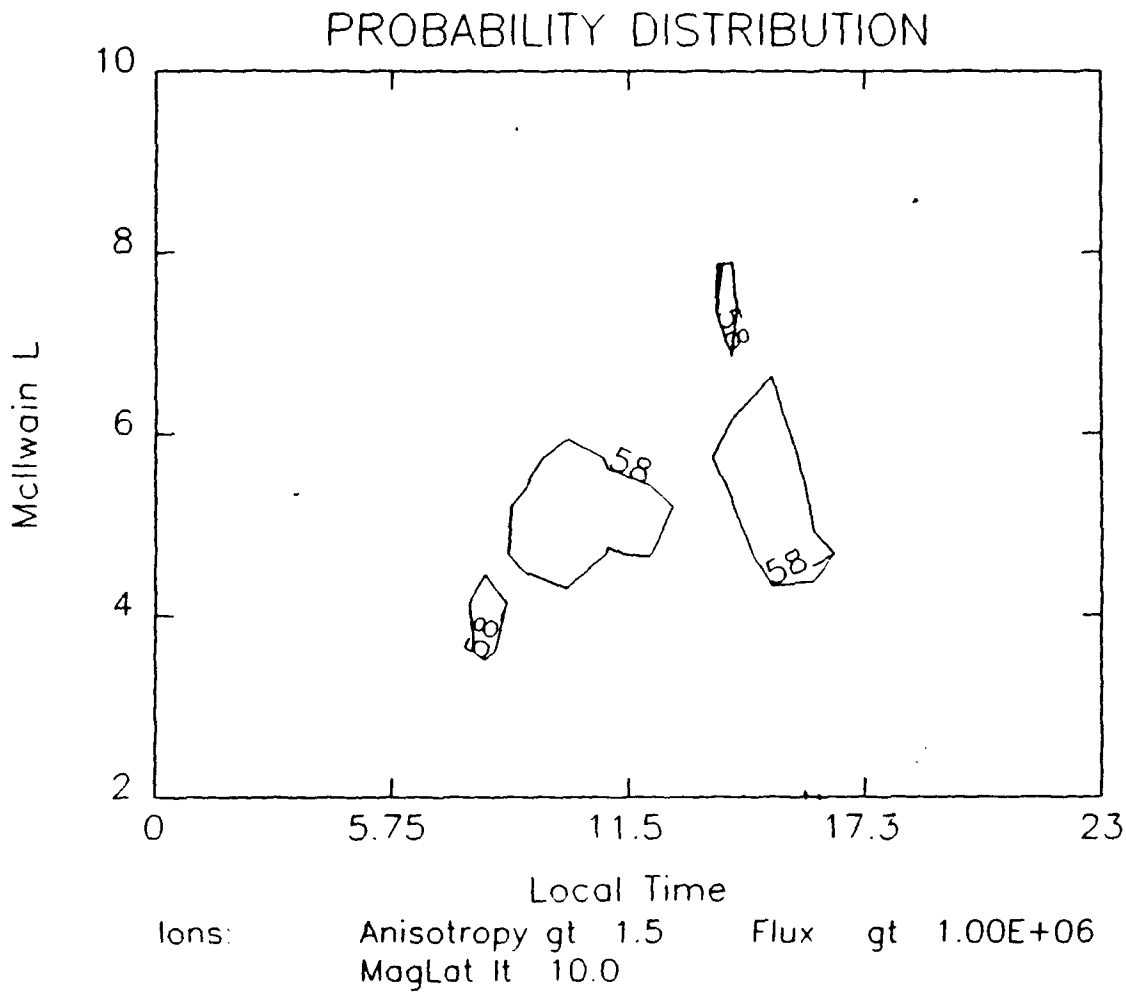

Figure 39. 58% Ion Probability Contour

region with the majority being just inside the boundary. Therefore, if the trapped ion distribution does occur along the plasmapause, then the trapped ions extend to higher altitudes as the plasmapause moves outward.

Figures 24 to 27 place the location of the peak probability to encounter trapped electrons in the dawn region centered at L = 6. The location of this probability peak is consistent with the initial observations by Olsen (1981) who also saw trapped electrons in the dawn to noon sector outside of the plasmapause.

In that paper, Olsen noted that the equatorially trapped electrons were observed in the presence of low energy (in the 30 - 70 eV range) field aligned electrons. By analogy, there were also, presumably, field aligned ion flows. This idea was expanded on by Olsen *et al.* (1987) to attempt to explain the filling process of the equatorial region with a trapped ion distribution. Figure 40 shows this process.

In this model, field aligned particles flow from the ionosphere out along the magnetic field lines. By this process the plasmapause region is filled. While in the process of filling the plasmapause, the particles are thermalized by shock processes along the field lines. This in turn leads to a heating region about the magnetic equator (Olsen *et al.*, 1987). But what drives this process to begin with? The most obvious answer is ambipolar diffusion.

By noting that the trapped electron distribution begins to grow at local dawn, it can be postulated that this filling process is driven by the polar wind. As the Sun's energy impinges on the Earth's atmosphere, photoelectrons are produced with energies of around 10 eV. Since these electrons are much lighter than ions, they are more likely to move out along the magnetic field lines.

This separation from the heaver ions (such as O^+) in the ionosphere results in an electric field pointing along the magnetic field lines. The force due to this electric

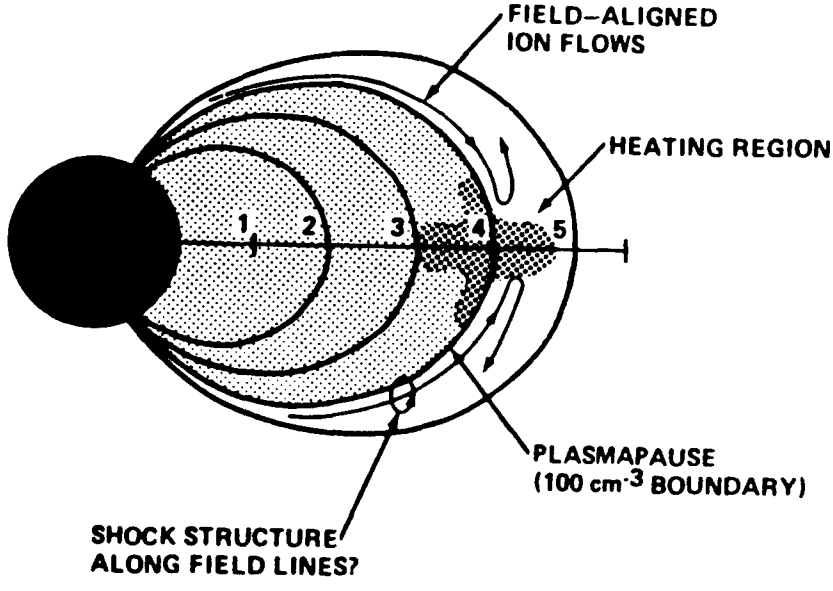

Figure 40. Plasma Heating at the Earth's Equator

field would result in the lighter ions (H^+ and He^+) being pulled up the field lines after the electrons. If the electrons undergo the same shock processes along the magnetic field lines as the ions do, then plasmasphere filling may be the process that results in the presence of both electron and ion trapped distributions. (Banks and Holzer, 1968)

Comparison of the ion and electron plots also may explain why the electron probability drops off by local noon. Figure 41a shows a contour plot of the probability distribution for electrons with the same selection criteria as in figure 24. Figure 41b shows ions with the same criteria as in figure 20. Figure 42 shows an over plot of the 60% probability contours from figures 41a and 41b.

If the probable presence of higher energy trapped ions, postulated earlier, is included, it can be seen that the high probability electron region ends at the boundary of the high probability ion region. Therefore, a result of the plasmapause increasing in L as the day progressed would be a saturation of the region of space where trapped electrons are usually seen with trapped ions. This ion saturation seems to, in turn, lead to a disruption in the process by which the trapped electrons are produced. More complete ion data will be needed to see if, in fact, this is the case.

Figures 30 and 31 show the probability distributions respectively for the ions and electrons found in the 0800 to 1200 time frame. This is the overlap region for high probability of occurrence for both trapped ion and electron distributions. Notice that the electron probability distribution drops off suddenly as it enters the region of high ion probability. The ion distribution behaves in the same manner when entering the region of high electron probability. This strengthens the conclusion that the electron and ion distributions do not normally occur in the same region of space and may in fact be mutually exclusive.

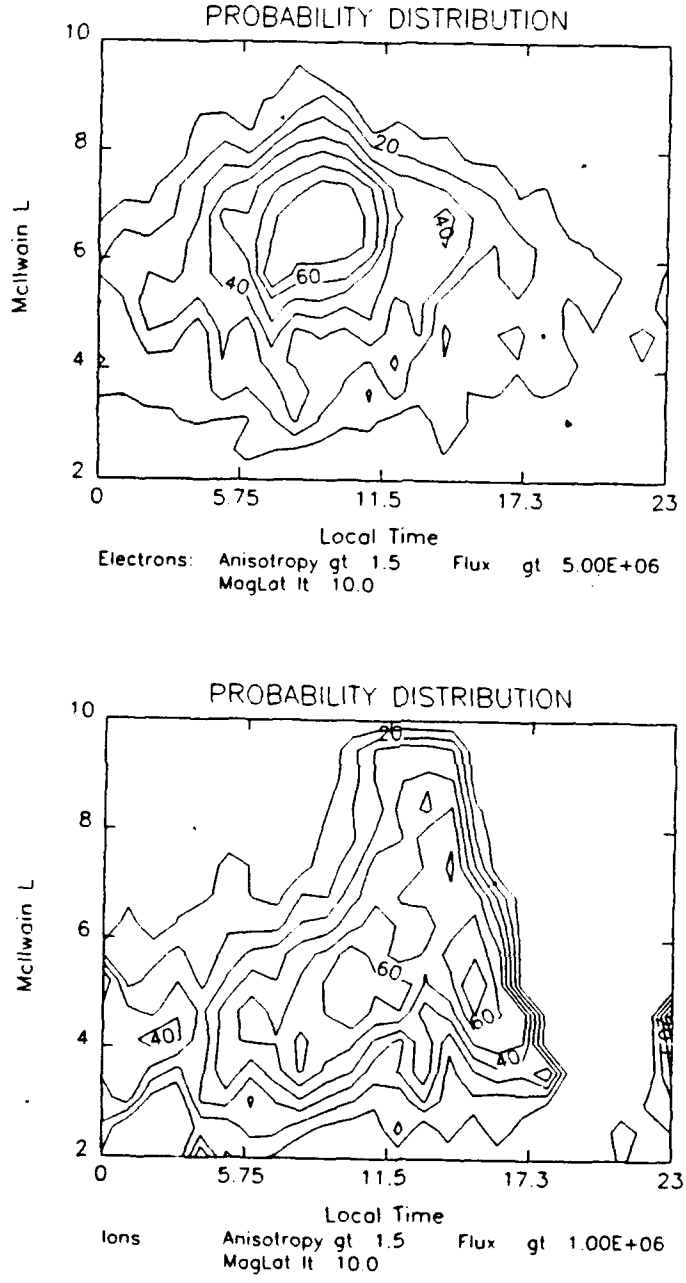

Figure 41. Ion and Electron Probability Contours

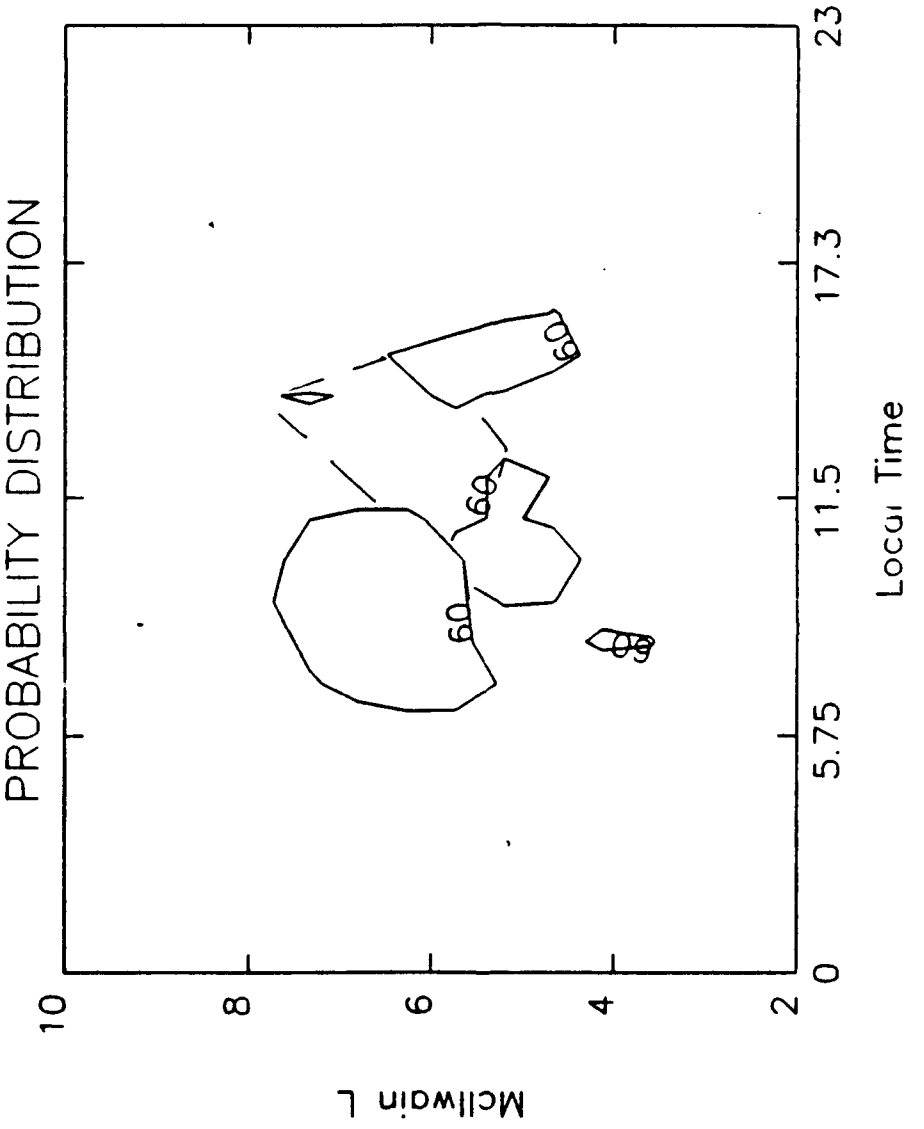

Figure 42. Probability Contours Overplot

For the 55 events listed in TABLE 2, 89% of the trapped ion distributions peak at a lower, or equal, L value than that of their related trapped electron distributions. This difference in latitude again strengthens the conclusion that equatorially trapped ion and electron distributions do not normally occur in the same place or at the same local time. Therefore, the general results of the survey are also seen strongly on a daily basis.

V. CONCLUSIONS

The location of the equatorially trapped plasmas are species dependant. The ions and electrons show a different local time dependance in the location of their occurrence probability peak. Electrons show a uniform high probability distribution centered at 0900 local time and an L value of 6. The fact that trapped electrons begin to be seen at local dawn lead to speculation that their existence is dependent on photoelectron emission from the Earth's ionosphere. The shape of this distribution is basically conical, however, it drops off more rapidly than it increases, with respect to local time.

Ions, meanwhile, have a probability distribution that shows a strong L dependence on local time. The high trapped ion probability region begins at local dawn, for L approximately 4, and rises to a maximum at between 1400 and 1500 local time with an L value of 8. The distribution then drops quickly in altitude as local time is increased. Additionally, there is a region of decreased probability in the afternoon sector for this data that is probably inhabited by higher energy ions.

The over all shape of the high trapped ion probability region mirrors that of the location of the plasmapause. This suggests that the trapped ion distribution is linked to the plasmapause. This would confirm Horwitz *et al*'s (1981) observations that 'pancake' distributions often occur in the vicinity of the plasmapause.

Additionally, it has been observed that trapped electrons seem to be excluded from regions of high trapped ion probabilities and visa versa. If the trapped ions actually do occur at the plasmapause, then as the altitude of the plasmapause rises, in the course of a day, this exclusion would effectively create a barrier that restricts the trapped electron distribution to the dawn to noon sector.

The survey work needs to be extended. It should take data from the next higher ion and electron channels (centered at 240 and 340 eV respectively). Such a survey would help to resolve whether higher energy ions do inhabit the region of decreased probability from 1200 to 1400 local time. The electron survey would ensure that the trapped distribution is not being underevaluated and that the location and shape of the trapped distribution presented in this paper is accurate.

In conclusion, it must be stated that more ion data are needed to obtain a compete picture of the trapped ion distribution. In previous surveys ions were only analyzed between L values of 2 and 5 for trapped ions. In this paper it has been seen that trapped ion distributions extend out to L = 8. However, due to the failure of the AMPTE/CCE ion-mass spectrometer, the dawn to dusk region was not surveyed for this paper. There therefore is a large gap in our knowledge on the behavior of trapped ions at higher altitudes.

REFERENCES

Acuña, M. H., Ousley, G. W., McEntire, R. W., Bryant, D. A., and Paschmann, G., "Editorial: AMPTE-Mission Overview," *IEEE Transactions on Geoscience and Remote Sensing*, vol. GE-23, no. 3, pp. 175-176, May 1985

Banks, P. M. and Holzer, T. E., "The Polar Wind," *Journal of Geophysical Research*, vol. 73, no. 21, pp. 6846-6854, 1 November 1968

Chappell, C. R., Harris, K. K., and Sharp, G. W., "The Morphology of the Bulge Region of the Plasmasphere," *Journal of Geophysical Research*, vol. 75, no. 19, pp. 3848-3861, 1 July 1970

Comfort, R. H. and Horwitz, J. L., "Low Energy Ion Pitch Angle Distributions Observed on the Dayside at Geosynchronous Altitudes," *Journal of Geophysical Research*, vol. 86, no. A3, pp. 1621-1627, 1 March 1981

Dassoulas, J., Margolies, D. L., and Peterson, M. R., "The AMPTE CCE Spacecraft," *IEEE Transactions on Geoscience and Remote Sensing*, vol. GE-23, no. 3, pp. 182-191, May 1985

Glasstone, S., *Sourcebook on the Space Sciences*, D. van Nostrand Company, Inc., 1967

Gurnett, D. A., "Plasma Wave Interactions With Energetic Ions Near the Magnetic Equator," *Journal of Geophysical Research*, vol. 81, no. 16, pp. 2765-2770, 1 June 1976

Harris, K. K., Sharp, G. W., and Chappell, C. R., "Observations of the Plasmapause from OGO 5," *Journal of Geophysical Research*, vol. 75, no. 1, pp. 219-224, 1 January 1970

Horwitz, J. L., "Major Questions on the Interchange of Thermal Plasmas Between the Ionosphere and Plasmasphere," *Journal of Atmospheric and Terrestrial Physics*, vol. 45, no. 11, pp. 765-775, 1983

Horwitz, J. L., Baugher, C. R., Chappell, C. R., Shelly, E. G., and Young, D. T., "Pancake Pitch Angle Distributions in Warm Ions Observed With ISEE 1," *Journal of Geophysical Research*, vol. 86, no. A5, pp. 3311-3320, 1 May 1981

Horwitz, J. L. and Chappell, C. R., "Observations of Warm Plasma in the Dayside Plasma Trough at Geosynchronous Orbit," *Journal of Geophysical Research*, vol. 84, no. A12, pp. 7075-7090, 1 December 1979

Klumpar, D. M. and Shelley, E. G., "Equatorially Trapped Light Ions at the Plasmapause/Ring Current Interface," *EOS*, vol. 67, p. 1154, 1986

Kurth, W. S., Craven, J. D., Frank, L. A., and Gurnett, D. A., "Intense Electrostatic Waves Near the Upper Hybrid Resonance Frequency," *Journal of Geophysical Research*, vol. 84, no. A8, pp. 4145-4164, 1 August 1979

Parks, G. K., *Physics of Space Plasmas*, Addison-Wesley Publishing Company, 1991

Olsen, R. C., "Equatorially Trapped Plasma Populations," *Journal of Geophysical Research*, vol. 86, no. A13, pp. 11,235-11,245, 1 December 1981

Olsen, R. C., "The Density Minimum at the Earth's Magnetic Equator," *Journal of Geophysical Research*, in press 1992

Olsen, R. C., Shawhan, S. D., Gallagher, D. L., Green, J. L., Chappell, C. R., and Anderson, R. R., "Plasma Observations at the Earth's Magnetic Equator," *Journal of Geophysical Research*, vol. 92, no. A1, pp. 2385-2407, 1 March 1987

Sagawa, E., Yau, A. W., and Whalen, B. A., "Pitch Angle Distributions of Low-Energy Ions in the Near-Earth Magnetosphere," *Journal of Geophysical Research*, vol. 92, no. A11, pp. 12,241-12,254, 1 November 1987

Shelly, E. G., Ghielmetti, A., Hertzberg, E., Battel, S. J., Altwegg-von Burg, K., and Balsiger, H., "The AMPTE/CCE Hot Plasma Composition Experiment (HPCE)," *IEEE Transactions on Geoscience and Remote Sensing*, vol. GE-23, no. 3, pp. 241-245, May 1985

Williams, D. V., Rycroft, M. J., Smith, A. J., Bezrukikh, V. V., Gringauz, K. I., Maynard, N. C., Morgan, M. G., and Thomas, T. W., "Intercomparison of Various Measurements of Thermal Plasma Densities At and Near the Plasmapause," *Advances in Space Research*, vol. 1, pp. 235-238, 1981

INITIAL DISTRIBUTION LIST

		No. Copies
1.	Defense Technical Information Center Cameron Station Alexandria, Virginia 22314-6145	2
2.	Library, Code 52 Naval Postgraduate School Monterey, California 93943-5100	2
3.	Department Chairman, Code Ph Department of Physics Naval Postgraduate School Monterey, CA 93943-5000	2
4.	Dr. R. C. Olsen, Code Ph/Os Department of Physics Naval Postgraduate School Monterey, CA 93943-5000	2
5.	Dr. D. M. Klumpar Dept. 91-20 Bldg. 255 Lockheed Palo Alto Research Laboratory 3251 Hanover St. Palo Alto, CA 94304	1
6.	Dr. T. E. Moore NASA/MSFC/ES53 Huntsville, AL 35812	1

7. Dr. J. L. Horwitz — 1
CSPAR
University of Alabama
Huntsville, AL 35899

8. Dr. N. Singh — 1
Department of Electrical Engineering
University of Alabama
Huntsville, AL 35899

9. Mr. F. Joiner — 1
Code 1114SP
Office of Naval Research
800 N. Quincy St.
Arlington, VA 22217

10. LT L. Scott — 1
3805 Eunice Hwy.
Hobbs, NM 88240

11. LT P. G. Braccio — 1
10 Brookside Dr.
Apt. 2E
Greenwich, CT 06830